Garnet amphibolite in the internal Eastern Segment, Sveconorwegian Province: monitors of metamorphic recrystallization at high temperature and pressure during Sveconorwegian orogeny

Tove Hernnäs

Dissertations in Geology at Lund University,
Master's thesis, no 553
(45 hp/ECTS credits)

Department of Geology
Lund University
2018

Garnet amphibolite in the internal Eastern Segment, Sveconorwegian Province: monitors of metamorphic recrystallization at high temperature and pressure during Sveconorwegian orogeny

Master's thesis

Tove Hernnäs

Department of Geology
Lund University
2018

Contents

Cover Picture: Migmatitic garnet amphibolite from Vickelsbo, Sweden. Photo: T. Hernnäs

Garnet amphibolite in the internal Eastern Segment, Sveconorwegian Province: monitors of metamorphic recrystallization at high temperature and pressure during Sveconorwegian orogeny

TOVE HERNNÄS

Hernnäs, T., 2018: Garnet amphibolite in the internal Eastern Segment, Sveconorwegian province: monitors of metamorphic recrystallization at high temperature and pressure during Sveconorwegian orogeny. *Dissertations in Geology at Lund University*, No. 553, 41 pp. 45 hp (45 ECTS credits).

Abstract: The analyzed area exposes a deep underthrusting lower plate of the Sveconorwegian orogen and facilitates studying of an elsewhere hidden portion of the Earth. Petrographic and structural studies of different metamorphic rock types within the southern Eastern Segment, Sveconorwegian Province, Sweden, were carried out to better understand the regional metamorphism and deformation history. The analyzed rock types are migmatitic garnet amphibolite, migmatitic garnet poor amphibolite, quartz feldspar rich gneisses and metagranites, leucocratic granitic gneiss and coronitic metagabbro.

Analyzed microtextures within the metagabbroic rock include coronitic textures. Such textures reveal the metamorphic history of the rocks and implies solid-state reactions forming such prominent coronites. Furthermore, penetrative coronitic texture together with a preserved igneous texture in metagabbroic rocks is an indicator of high -grade metamorphism in dry conditions, reaching granulite facies. Previous studies imply that the coronitic metagabbro and the migmatitic garnet amphibolite have an identical protholith, and that such can be traced throughout the Eastern Segment. The relict igneous texture of the coronitic metagabbro confirms dry conditions within the rock complex. Fluids did not percolate the system and the reactions where therefore inhibited and did not run to completion.

Additionally, a regional scale fold within the garnet amphibolite, with the coronitic metagabbro located in the hinge zone, is suggested to cause a lack of fluid percolation due to deformational differences. Differences in deformation and metamorphism may be affected by folding as the hinge zone can be less deformed than the limbs of the fold. Conclusively, the coronitic metagabbro with its peculiar texture has been of substantial importance to monitor the metamorphic conditions and recrystallization processes. It supports previous studies within the region, that the rocks experienced high-grade metamorphism and deformation.

Keywords: Sveconorwegian, Metamorphic petrology, Mapping, Coronitic metagabbro, Microtextures, Eastern Segment.

Supervisor(s): Charlotte Möller

Subject: Bedrock Geology

Tove Hernnäs, Department of Geology, Lund University, Sölvegatan 12, SE-223 62 Lund, Sweden. E-mail: tove.hernnaes@gmail.com

Granatamfibolit i inre Östra Segmentet, Svekonorvegiska provinsen: bevisning för metamorf rekristallisering vid höga temperaturer och högt tryck under den Svekonorvegiska orogenesen.

TOVE HERNNÄS

Hernnäs, T., 2018: Granatamfibolit i inre Östra Segmentet, Svekonorvegiska provinsen: bevisning för metamorf rekristallisering vid höga temperaturer och högt tryck under den Svekonorvegiska orogenesen. *Examensarbeten i geologi vid Lunds universitet*, Nr. 553, 41 sid. 45 hp.

Sammanfattning: Det undersökta området blottar en djupare del av den underskjutande undre kontinentalplattan som är en del av den Svekonorvegiska orogenesen och möjliggör studier av en normalt dold del av en orogenes. Petrografi- och strukturstudier av metamorfa bergarter inom den södra delen av det Östra Segmentet, Svekonorvegiska provinsen, Sverige, genomfördes för att bättre förstå den regionala metamorfosen och tidigare deformationer. Undersökta bergarter inkluderar migmatitisk granatamfibolit, migmatitisk granatfattig amfibolit, kvarts-, feldspatrika gnejser och metagraniter, leukokratiska granitiska gnejser och koronitisk metagabbro.

Analyserade mikrotekturer inom den metagabbroida bergarten innefattar koronitiska texturer. Sådana texturer avslöjar berggrundens metamorfa historia och antyder på förening i fast fas. Genomgående koronitiska texturer tillsammans med en bevarad vulkanisk textur i metagabbroida bergarter är en indikator på en hög metamorf grad i torra förhållanden som uppnått granulit facies. Tidigare studier visar på att den koronitiska metagabbron och den migmatitiska granatamfiboliten har en gemensam protolit och att denna kan spåras över hela det Östra Segmentet. Den bevarade vulkaniska texturen i den koronitiska metagabbron är ett bevis på torra förhållanden inom berggrunds komplexet eftersom fluider inte perkolerade och reaktionerna avstannade.

Ett regionalt veck i granatamfiboliten, där den koronitiska metagabbron är belägen i veckzonen kan tyda på att fluider inte kunnat tränga in och veckstrukturen har därför i sin tur påverkat berggrunden olika. Ett veck är både komprimerat och utsträckt i veckzonen och detta kan leda till förändringar i fluider som sedan har stor inverkan vid metamorfos. Den särskilda texturen hos den koronitisk metagabbron har varit en betydande faktor för att förstå de metamorfa förhållandena som påverkat området. Studien styrker tidigare forskning i området och visar på att berggrunden påverkats av höggradig metamorfos och deformation.

Nyckelord: Svekonorvegisk, Metamorf Petrologi, Kartering, Coronitisk metagabbro, Mikrotexturer, Östra Segmentet

Handledare: Charlotte Möller

Ämnesinriktning: Berggrundsgeologi

Tove Hernnäs, Geologiska institutionen, Lunds Universitet, Sölvegatan 12, 223 62 Lund, Sverige. E-post: tove.hernnaes@gmail.com

1 Introduction

The internal section of the Eastern Segment, Sveconorwegian Orogen, Scandinavia, offers an investigation of the Baltica continent that has been metamorphosed at high temperatures and pressures (e.g., Möller, 1998; Andersson, et al., 1999; Söderlund, et al., 2002; Möller, et al., 2007; 2015; Tual, et al., 2015; Tual, et al., 2017; Möller & Andersson, 2018). One interesting aspect of this area is that it exposes a deep part of the underthrusting lower plate of the Sveconorwegian Orogen (Möller & Andersson, 2018). The Eastern Segment exposes the same crust, from unmetamorphosed in the east, to high-pressure granulite-facies in the west (op cit.; Möller et al., 2015) (Fig. 1).

As the deeper section of a continental collision is studied correlations can be drawn to young, ongoing continental collision zones, such as the Indian- and Eurasian plate forming the Himalayas. This contributes to an overall better understanding of continental collision zones. Furthermore, reconstructions of the lithospheric plates are facilitated as the plate dynamics are better understood. As the deformational events within the affected areas have been carefully studied the plate dynamics can be better understood as well.

This study aims for a greater understanding of the metamorphic variations in the southern parts of the Eastern Segment. Mapping of a 25 km^2 area (scale 1:10,000; Fig. 2) near the town of Burseryd was carried out to document the structural and metamorphic relationships between and within the different rock types. The structures, textures and mineral assemblages of metagabbroic rocks and migmatitic orthogneisses have been used as monitors of metamorphic recrystallization under high temperature and pressure conditions.

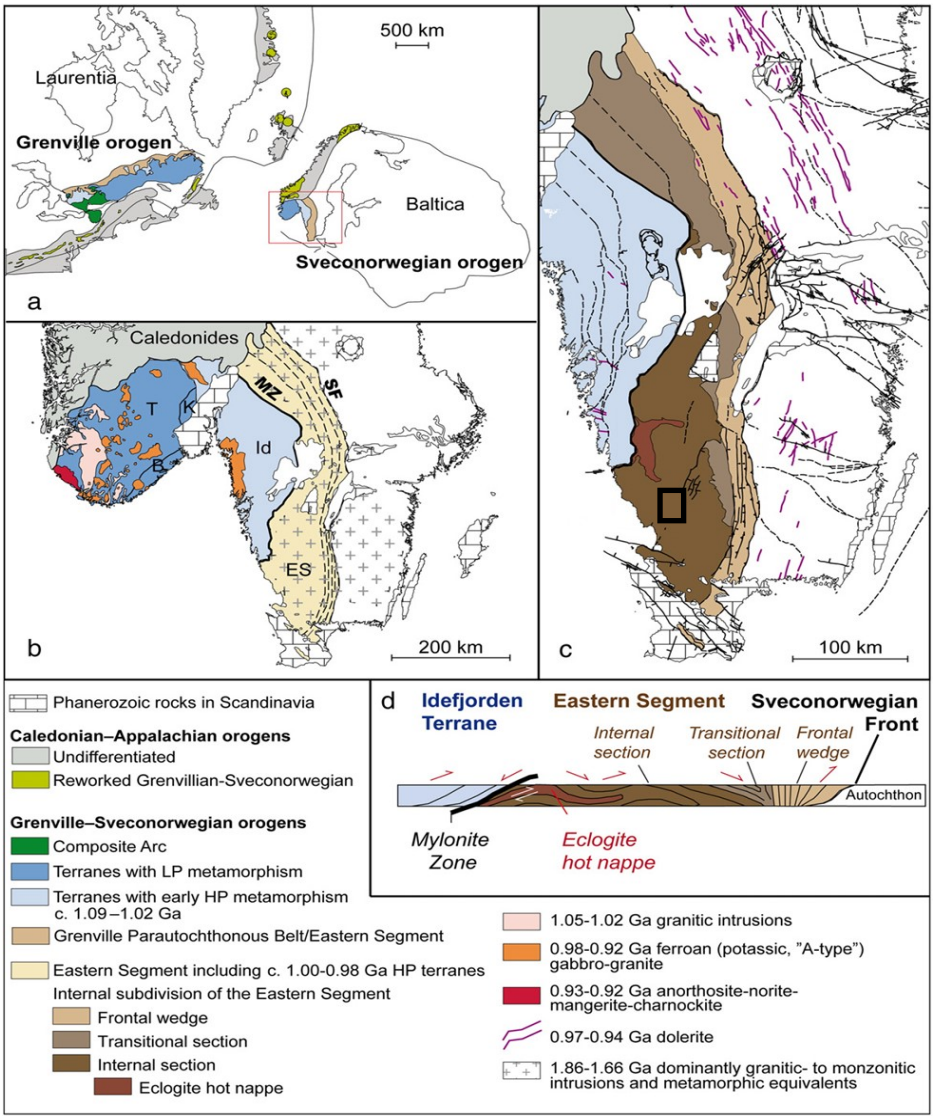

Fig. 1. Regional and tectonic setting. Figures from Möller et al. (2015) with permission from Elsevier. (a) Possible configuration of continents at the end of the Grenvillian-Sveconorwegian orogeny. (b) Tectonic map of the Sveconorwegian Province with the main lithotectonic units. (c) Tectonic subdivisions of the Eastern Segment. Black box indicates study area. (d) Simplified vertical section across the Eastern Segment from W to E.

2 Regional context

2.1 The Sveconorwegian orogen

The Sveconorwegian Province is the deeply eroded remnants of a mountain belt that formed during accretion and continental collision, 1.14–0.92 Ga (Bingen et al., 2005; Bingen et al., 2008). It is commonly assumed to have involved collision with another, unidentified, craton, as the supercontinent Rodinia formed (op. cit.; Li et al., 2008). The Sveconorwegian Province is the analogue to the Grenville Province in North America, which share a similar first-order architecture and timing of orogenic stages (Möller, et al., 2015; 2018, and references therein) (Fig. 1a). Paleomagnetic and geochronological data are combined with stratigraphic correlations in order to reconstruct the Late-Precambrian supercontinent Rodinia (Li et al., 2008 and references therein). The timing of continental collision between the Baltica plate (Eastern Segment) and the western Sveconorwegian terranes, or the unidentified continent, is best dated by the age of eclogite-facies metamorphism and associated tectonic burial of the Eastern Segment at 990-970 Ma (Möller et al., 2015).

Another hypothesis, proposed by Slagstad et al., (2013), implies that the Sveconorwegian Orogen was formed by a non-collisional accretion. This neglects several features of the Sveconorwegian orogen, such as the crustal underthrusting caused by the collision, the high-grade metamorphism and penetrative deformation affecting the Eastern Segment at 0.98-0.97 Ga and the presence of the 0.99 Ga eclogite-bearing nappe (Möller & Andersson, 2018).

The Sveconorwegian orogen is divided into a Paleoproterozoic Eastern Segment and four main terrains delimited by major shear zones: Idefjorden, Kongsberg, Bamble and Telemarkia terrains (Bingen et al., 2008) (Fig. 1b). The Mylonite zone forms the west-dipping tectonic boundary of the Eastern Segment with the Idefjorden terrane (e.g., Möller et al., 2007; Möller & Andersson, 2018) (Fig. 1a and b). The eastern limit is marked by a subvertical deformation zone, the Frontal Wedge, characterized by non-penetrative deformation and metamorphism, and by lower amphibolite- to greenschist-facies metamorphism (Fig. 1b and d). These zones are north-south trending and orogen parallel.

The chemical compositions and protolith ages (1.73-1.66 Ga) of the gneisses in the Eastern Segment show that they are metamorphosed equivalents of the TIB rocks farther east (e.g. Connelly et al., 1996; Andersson et al., 2002; Söderlund et al., 2002; Möller et al., 2007; 2015; Pinan-Llamas et al., 2015). The TIB rocks intruded 1.85-1.65 Ga (Högdahl et al., 2004; Noltre et al., 2011; Petersson et al., 2013; Stephens & Andersson, 2015). Geographically the undeformed TIB rock are located east of the Eastern Segment and crosscut by at least three generations of 1.58-0.94 Ga dolerite dykes (Söderlund et al., 2005) (Fig. 1c).

The Sveconorwegian metamorphism within the Eastern Segment overprints earlier Mesoproterozoic, Hallandian, metamorphic effects and intrusions, which have been dated 1.47–1.38 Ga (Hubbard 1975; Christoffel et al., 1999; Söderlund et al., 2002; Möller et al., 2007; Ulmius et al., 2015). The Hallandian event is considered an orogenic event, with migmatization and low-pressure metamorphism reaching the upper amphibolite facies, as recorded by metamorphic zircon (op. cit). Metamorphic zircons from multiple generations give evidence for Sveconorwegian high-pressure amphibolite-, high-pressure granulite-, and eclogite-facies metamorphism, and migmatization, between 1006 ± 68 Ma and 934 ± 6 Ma (Möller & Andersson, 2018 and references therein).

2.2 The southern Eastern Segment

The metamorphic grade within the Eastern Segment increases southwestwards, reaching upper amphibolite-facies and high-pressure granulite-facies. The southwest area is characterized by deformed orthogneisses, garnet-poor and garnet-rich amphibolites, and mafic high-pressure granulites (Johansson et al., 1991; Johansson & Kullerud, 1993; Wang & Lindh, 1996; Möller 1998; Söderlund et al., 1999; Austin Hegardt et al., 2005; Möller & Andersson, 2018 and references therein). Rocks in the southern parts of the Eastern Segment are predominantly migmatitic (e.g., Andersson et al., 1999; Söderlund et al., 1999; Möller et al., 2007; Hansen et al., 2015; Pinan-Llamas et al., 2015). Partly retrogressed eclogites occur in a separate terrane (Möller et al., 2015; Tual et al., 2015; Fig 1). Metamorphic peak conditions of the eclogites are estimated at 870 °C and 18 kbar (Tual et al., 2017). U-Pb zircon dating of the eclogites, at the locality Ammås, give ages of 1000 – 970 Ma (Andersson et al., 2017).

Aeromagnetic anomaly maps provide data to aid the interpretations of geological and structural elements within the Eastern Segment. A high-resolution airborne magnetic survey conducted by the Geological Survey of Sweden (SGU) help to distinguish large scale features such as foliation, folds, and shear zones regionally within the Eastern Segment. The banded pattern in the magnetic maps reflects the tectonic banding of alternating gneisses and metabasites and, in outcrop scale, the migmatitic or gneissic structures (e.g., Möller et al., 2007).

3 Methods

Geological mapping at a scale of 1: 10,000 was performed during 4 weeks in the period between September and October 2017. The study area is located in the region of Småland in Sweden, north of the town Broaryd. The mapped area has a total area of 25 km^2 (Fig. 2). Observations and documentation of rock types and structures were conducted at 96 localities, listed in Appendix I and II. Most localities were marked using a Garmin Oregon instrument and the gathered Global Positioning System (GPS) data reported in the SWEREF 99TM (Swedish reference frame 1999) geodetic reference system. Hand samples from 25 localities were taken for closer inspection. The regional-scale bedrock map of Jönköpings county, in 1: 250,000 scale published by the Swedish Geological Survey (Wik et al., 2007), were used together with base maps and observational points in 1: 50,000 scale from the Swedish Geological Survey. Thin sections, provided by SGU and Victoria Beckman, were analyzed using polarized microscopy using a Nikon

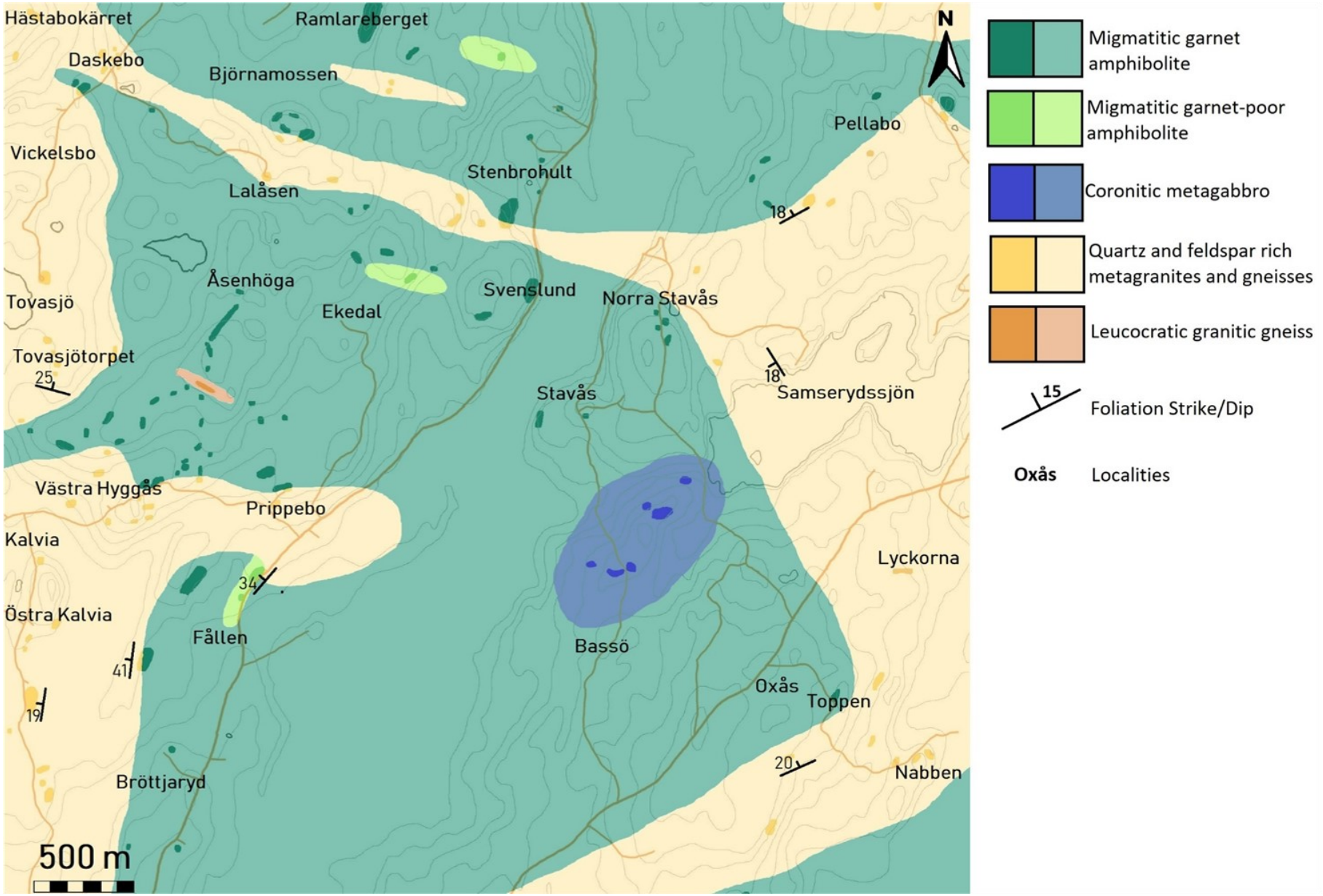

Fig. 2. Geological bedrock map in the scale 1:10,000 (this work). Saturated hues mark observed outcrops.

eclipse E400 POL fitted with a Luminera Infinity 1-2CB camera for photomicrographs. Selected thin sections were analyzed with a scanning electron microscope (TeScan SEM) linked with an energy-dispersive X-ray analysis system (EDS; Oxford Instruments), at the Department of Geology, Lund University, Sweden.

The terminology used to describe migmatites in this paper is proposed by the Sub-Committee on the systematics of Metamorphic Rocks (SCMR), which is a sub-committee to the International Union of Geological Sciences (IUGS) Commission on the Systematics in Petrology (CSP). The SCMR terminology uses non-genetic descriptive terms. The descriptive terms used in this paper are leucosome, melanosome and mesosome. The leucosome is defined as the light-colored, coarser-grained layers, veins or pods. Melanosome is defined as the dark component of the rocks, with a schistose appearance. Lastly, the mesosome refers to the intermediate component between leucosome and melanosome (Winter, 2014). The mineral composition of anorthitic plagioclase is based on the following calculation: An = 100*Ca/(Ca+Na+K). Similarly, the composition of almanditic garnet is based on the following calculation: Alm = 100*Fe2+ /(Ca+Fe2++Mg+Mn). Mineral compositions are calculated using the mol.%. The mineral analyses are normalized to 100 wt.% oxides, except for hornblende with a normalization value of 98 wt.% oxides. Mineral names are abbreviated in photomicrographs for simplicity, according to Kretz (1983).

4 Results

4.1 Rock types in the Broaryd area

Previously conducted mapping in the area, by SGU, in scale 1: 250,000 and reported in Wik et al., (2007), concluded that the rock types in the Broaryd area include leucocratic metagranitic gneiss, granitic to quartz-monzonitic migmatitic gneiss, migmatitic garnet amphibolite and garnet-rich mafic granulite.

Mapping during this study resulted in more detailed description of the distribution and variation of different rock types in the area. The area is composed of five main rock types, all of which are high-grade metamorphic rocks: (1) migmatitic garnet amphibolite, (2) garnet-poor migmatitic amphibolite, (3) Quartz and feldspar rich metagranites and migmatitic gneisses, (4) leucocratic granitic gneiss, and (5) coronitic metagabbro. Original structures and textures of the protoliths are largely overprinted by metamorphism and deformation.

The geological map produced in this study is based on detailed study of 96 outcrops, including measured foliations, and is supported by data from aeromagnetic maps and published studies of the regional geology. Bright colored areas in Figure 2 represent outcrops. Comparisons between the published regional geological map 1: 250,000 (Wik et al., 2007) and results from the conducted mapping show that the correlations between the rock types have been interpreted differently. Previously unknown outcrops are one aspect that have caused the main traits of the geological map to diverge from the previous one. Data from aeromagnetic anomaly maps provide information on folds, as well as tectonic banding or distinct internal structures of the rocks (Appendix IV). In addition, measured foliations in felsic rocks have aided the interpretations of covered sections.

4.2 Migmatitic garnet amphibolite

This rock type is on average the most common exposed rock type within the mapped area. It predominates the western area of the map, although found throughout.

4.2.1 Macroscopic description

The matrix of migmatitic garnet amphibolite is generally medium grained and composed of amphibole, biotite, plagioclase, and minor quartz and opaque minerals. The garnet grains range in size from a couple of millimeters up to porphyroblasts two centimeters in diameter. The leucosome is often concentrated in smaller patches, in pressure shadows or in cm-thick veins. The leucosome consists of plagioclase and quartz, locally with small garnet or amphibole grains. Several smaller elongated mesosome domains often extend in the same direction. The plagioclase rich leucosome has in these occurrences migrated to the low-pressure sites bordering the competent garnet crystals (Fig. 3a). The abundance of garnet porphyroblasts vary greatly in different outcrops. Garnet porphyroblasts may be many and small or large and fewer at an outcrop scale.

A large outcrop located at Vickelsbo (BRO17006B) is of particular interest as macroscopic features can be easily studied. It is also the location of a clearly exposed contact between the migmatitic garnet amphibolite and the migmatitic orthogneiss (Fig. 4a). The garnet amphibolite is rich in both leucosome and decimeter thick leucocratic pegmatitic dykes. The outcrop is approximately 20 x 10 m and the garnet amphibolite is crosscut by several pegmatitic dykes oriented mainly in an E-W direction. The width of the pegmatitic dykes ranges from a couple of centimeters up to a few decimeters. The contacts with the host rock are sharp and undulous. The pegmatite is composed mostly of coarse grained plagioclase and quartz (Fig.

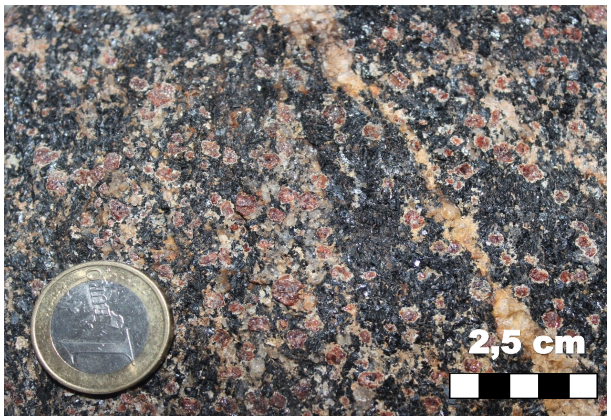

Fig. 3. Garnet-porphyroblastic migmatitic amphibolite. Outcrop at Kalvia (BRO10051B). Note the thin light-colored domains of feldspar around the garnet grains and the irregular quartz-feldspar leucosome veins.

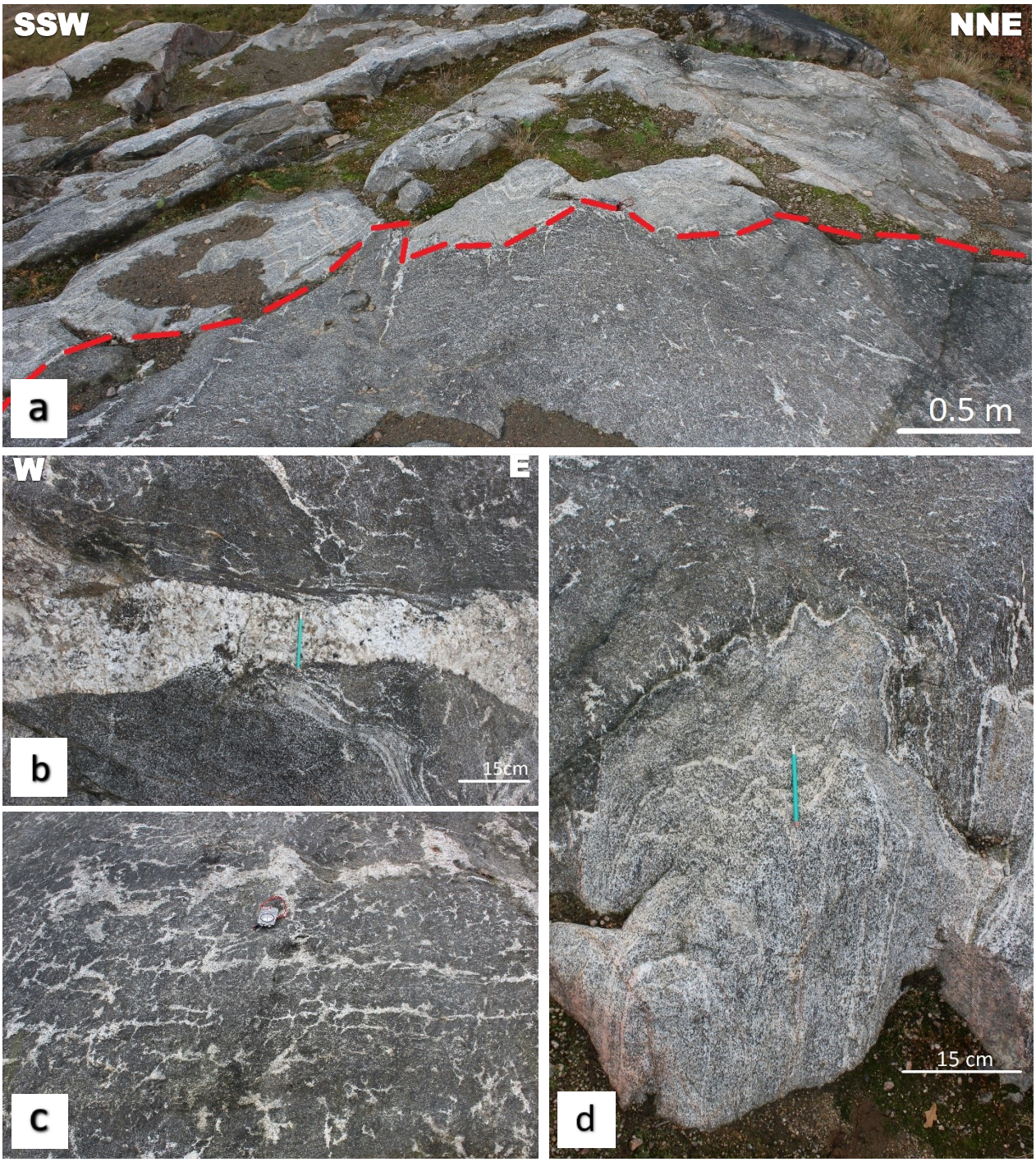

Fig. 4. Migmatitic garnet amphibolite at Vickelsbo (BRO17006). (a) View from the top of the outcrop towards the contact zone between garnet amphibolite and less mafic migmatitic orthogneiss. The contact is marked with a red line, where the lower dark grey surface is composed of migmatitic garnet amphibolite. (b) Pegmatitic dyke within the migmatitic garnet amphibolite. (c) Net-structured leucosome, composed of coarse-grained plagioclase and quartz, following two main directions. Garnet porphyroblasts within the mesosome are millimeter sized in this outcrop, amphibole is fine grained. (d) Close-up of the contact between the garnet amphibolite and the less mafic orthogneiss. A leucocratic vein is located at the contact. The grey migmatitic orthogneiss has a nearly vertical gneissic foliation striking in a N-S trend.

4b). The leucosome is mm- to cm-thick and have two preferred directions, indicative of two main weakness planes (Fig. 4c). Locally there is a thin melanocratic selvedge around the leucosome. This melanocratic selvedge is composed mainly of amphibole. A mm-thick leucosome vein along with a dark colored mafic border, towards the migmatitic garnet amphibolite, marks the contact between the two rock types (Fig. 4d).

Migmatitic amphibolite at Lalåsen (BRO17011A) has leucosome veins of up to 2 cm in diameter (Fig. 5a). Smaller patches of leucosome are

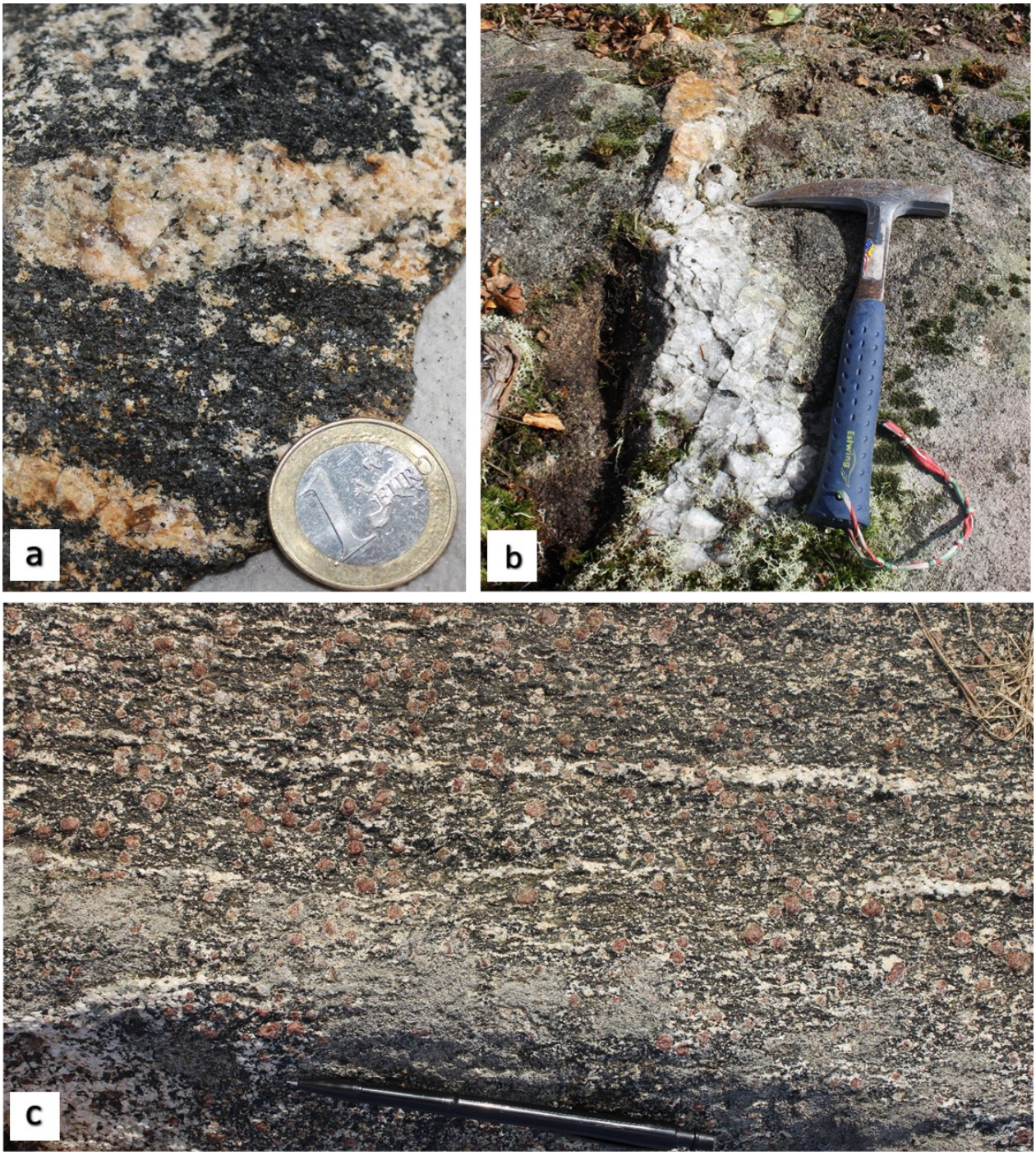

Fig. 5. Examples of different varieties of leucocratic veins in migmatitic amphibolites. (a) Sample from Lalåsen (BRO17010) devoid of garnet. The leucosome is composed mainly of quartz and feldspar and contains subordinate millimeter-sized garnet and biotite crystals. (b) At Norra Bröttjaryd (BRO17070) numerous irregular pegmatitic dykes crosscut the rock. The pegmatitic dykes are composed mostly of plagioclase and quartz (trondhjemitic composition). (c) Migmatitic garnet amphibolite at Svenslund (BRO17143) with numerous garnet porphyroblasts (red) and mm thick stromatic leucosome veins.

also found within the melanosome. The leucosome is composed of feldspar (mainly plagioclase) and quartz. Very coarse grained migmatitic veins crosscut the gneissic foliation of the migmatitic garnet amphibolite at Norra Bröttjaryd (BRO17070). At this locality a very coarse grained quartz vein with a grain size of up to five centimeters can be observed (Fig. 5b). Some outcrops, eg. at Svenslund (BRO17143), expose migmatitic garnet amphibolite with stromatic leucosome. The leucosome is whiteish and forms easily distinguishable millimeter thick bands within the rock (Fig. 5c).

4.2.2 Microtextures – polarized microscopy

Variations in grain size range from fine to medium

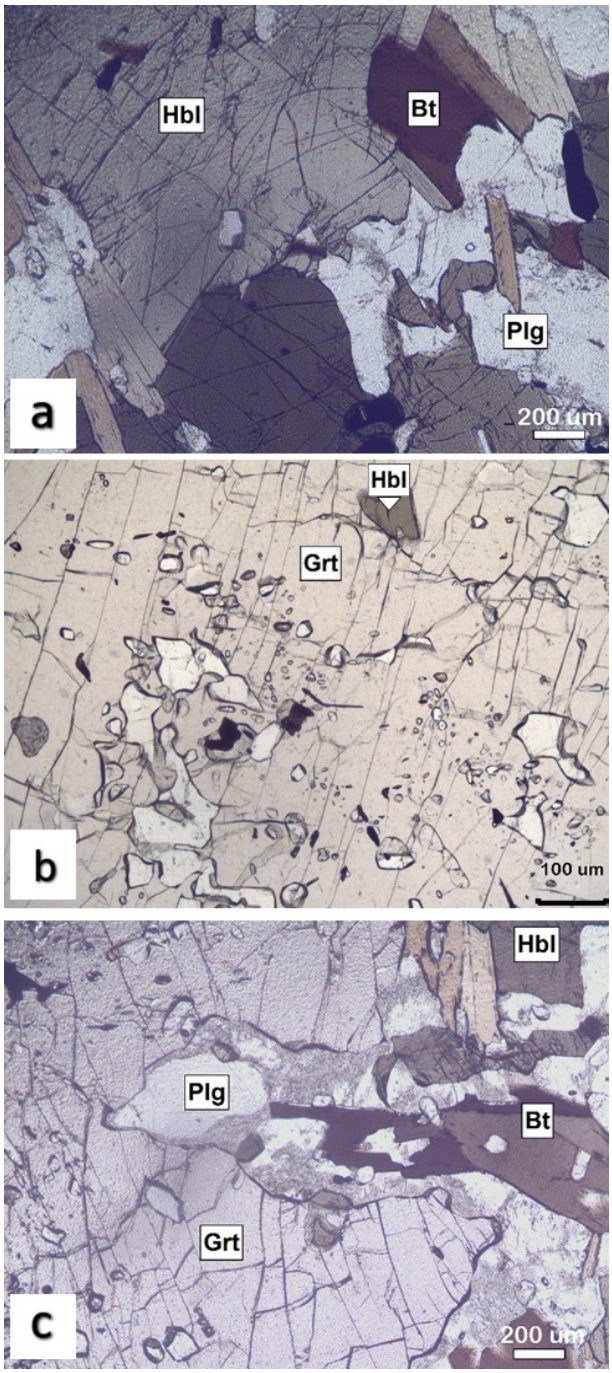

Fig. 6. Photomicrographs of migmatitic garnet amphibolite from Hålgryte (JAN040099B; all in plane polarized light, PPL). (a) Matrix melanosome minerals, comprising coarse grained olive-green hornblende, brown biotite laths and plagioclase. Up to 6 millimeters large garnet porphyroblasts are also present in the rock. (b) Poikiloblastic garnet grain with inclusions of primarily hornblende, plagioclase, quartz, titanite, rutile and opaques. (c) Plagioclase rim around garnet porphyroblast. The garnet has numerous inclusions in the core and fewer towards the rim of the crystal. Hornblende and biotite grains are also present in the section.

grained migmatitic garnet amphibolite (Fig. 6a). The mineral assemblage is hornblende, plagioclase, garnet, biotite, clinopyroxene, iron oxides and accessory minerals such as microcline, olivine, orthopyroxene, apatite, zircon and baddeleyite.

In the studied thin section of garnet amphibolite from Hålgryte (JAN040099B), subhedral garnet porphyroblasts up to 7 mm in diameter are distributed in a fine grained matrix of olive-green hornblende, plagioclase, biotite, and opaque minerals (mainly FeTi-oxide). The garnet grains are fractured and contain numerous inclusions of plagioclase, hornblende, biotite and accessory minerals such as titanite, apatite, rutile and opaques (Fig. 6b). Elongated biotite grains with a strong brown pleochroism are also featured within the same section (Fig. 6c).

4.3 Migmatitic garnet-poor amphibolite

Migmatitic garnet-poor amphibolite was found in three outcrops within the area. Migmatitic garnet-poor amphibolites occur solely in proximity to migmatitic garnet amphibolites.

4.3.1 Macroscopic description

The migmatitic garnet-poor amphibolite is medium grained, blackish, rich in amphibole and plagioclase, and devoid of or very poor in garnet. The migmatitic garnet-poor amphibolite locally contains small patches of leucosome composed of plagioclase and quartz. Foliation is weak in the mesosome, however elongated or tightly folded leucosome patches define the foliation of the rock (Fig. 7a).

At Stenbrohult and Fållen (BRO17020 and BRO17080B) the mineral assemblage is, apart from garnet, identical to that of the migmatitic garnet amphibolite described previously. At both localities, large quantities of quartz and plagioclase lenses and veins are present. At Stenbrohult (BRO17020), some of the quartz lenses are augen shaped and locally tightly folded. At Fållen (BRO17080B), the amphibolite is medium grained and has a striped appearance, with the leucocratic veins and lenses defining a pronounced gneissic foliation striking NNE-SSW (Fig. 7b).

4.3.2 Microtextures – polarized microscopy

The studied thin section of garnet-free amphibolite from Nenesmo (JAN040011B; Appendix III) has an uneven fine to medium grain size and consists of olive-green hornblende, plagioclase, biotite (largely altered), titanite, and opaque minerals. Hornblende grains are oriented, anhedral or subhedral, and have inclusions of opaques and plagioclase. Plagioclase grains are anhedral and have a dusty appearance due to very fine grained mica (sericite) and calcite. Titanite grains are anhedral to subhedral and form aggregates. The titanite grains have small inclusions of ilmenite and rutile (Fig. 8).

4.4 Quartz and feldspar rich metagranites and gneisses

Metagranites and gneisses compose the most abundant rock types within the mapped area. They vary in composition, thickness of gneissic layering or stromatic banding, strain, and presence/absence and style of meso- and macroscale folds. In small outcrops, the average composition is difficult to determine due to

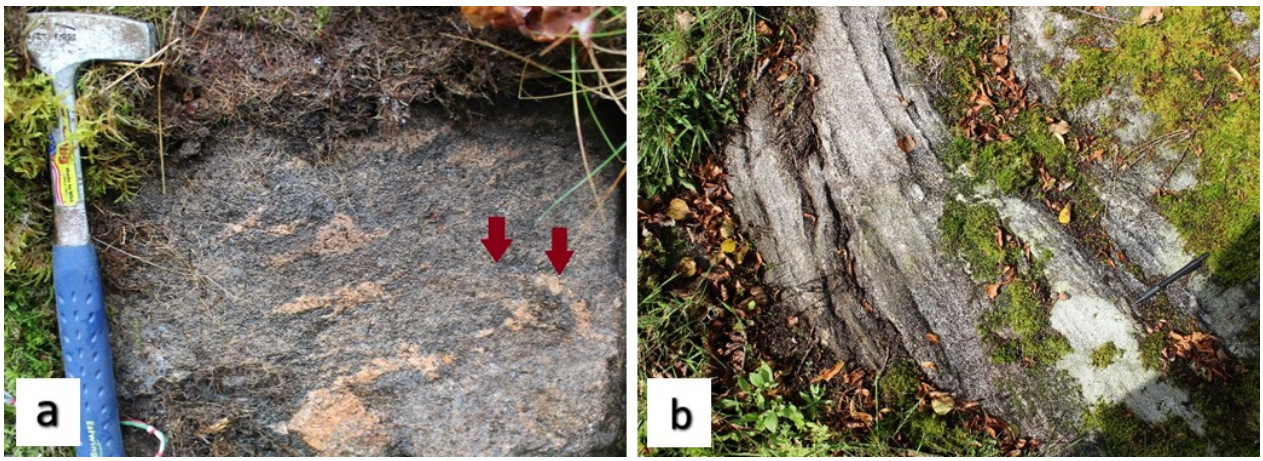

Fig. 7. Migmatitic garnet-poor amphibolite at Ekedal (BRO17027; a) and Fållen (BRO17080B; b). (a) Leucocratic patches are locally folded (red arrows); the veins appear pinkish due to weathering/alteration. (b) Medium-grained amphibolite with strong fabric defined by thin parallel quartz-rich leucosome veins.

the presence of gneissic layering (a grey migmatitic gneiss can be mistaken for the mesosome of a more K-feldspar rich gneiss).

4.4.1 Macroscopic description

Migmatitic gneisses contain feldspar, quartz, plagioclase, biotite, hornblende, and accessory minerals (mainly opaque minerals, titanite, apatite, and zircon). Layers and stromatic bands vary in thickness from cm- to m-scale, where stromatic leucosome is rich in quartz and feldspar, and dark-colored bands are richer in amphibole and biotite. K-feldspar and quartz rich varieties of the gneisses and metagranites have a pinkish appearance, often intercalated with millimeter thick dark colored bands rich in biotite and/or amphibole (Fig. 9a). The platy minerals, e.g. biotite, have a preferred orientation parallel with the gneissic foliation. The gneissic foliation is commonly folded (Fig. 9b and c).

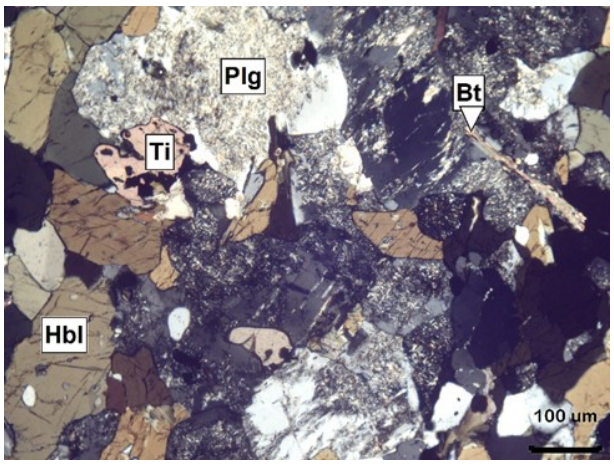

Fig. 8. Microphotograph of migmatitic garnet-poor amphibolite from Nenesmo (JAN040011B) in cross polarized light (XPL). The rock consists of hornblende, plagioclase (partly altered; sericite/saussurite and calcite), biotite, titanite and opaques, e.g. ilmenite inclusions in titanite.

At some localities distinct stromatic leucosome has a thin mafic selvedge. This can be seen at Östra Kalvia (BRO17083; Fig. 10a). The leucosome veins are cm-thick with a spacing of approximately five centimeters and make up approximately 20 volume-% of the rock. The leucosome is coarse grained and occurs in both patches and veins (Fig. 10b). The leucocratic veins are locally bordered with a mafic selvedge (Fig. 10a and b; red arrows). The veins are gently folded and not perfectly parallel.

In localities such as at Lalåsen (BRO17011A and B), the contact zone between garnet amphibolite and granitic gneiss is evident, even if it is not sharp. The granitic gneiss contains a few porphyroblasts of garnet, and the garnet amphibolite contains more abundant leucocratic veins. At other localities within the mapped area the contact zones are sharp. At Lalåsen (BRO170035) a medium grained leucocratic granitic gneiss is hosted within the garnet amphibolite and the outcrop is approximately a few hundred meters long and five meters wide. The leucocratic granitic gneiss is pinkish with abundant K-feldspar and quartz (Fig. 10c). The minerals are not strained, nor is there any prominent foliation. The contact with the surrounding garnet amphibolite is difficult to observe due to dense vegetation. The rock type exposed at Lalåsen (BRO17035) forms a protruding morphology. It is interpreted to be a light reddish medium-grained leucocratic granitic gneiss, similar to that previously found at NE. Ullared (6349724/1336749; Mårdaklev type granite) (Wik et al., 2007).

Folding of a mafic biotite-rich sliver has been recorded in a felsic migmatitic gneiss, at Nabben (BRO17086; Fig. 11a). Locally within this area, coarse grained crosscutting pegmatitic dykes occur. At Pellabo (BRO17103), there is a sharp contact between the medium grained host gneiss and the very coarse grained pegmatitic dyke (Fig. 11b; red line). The dyke

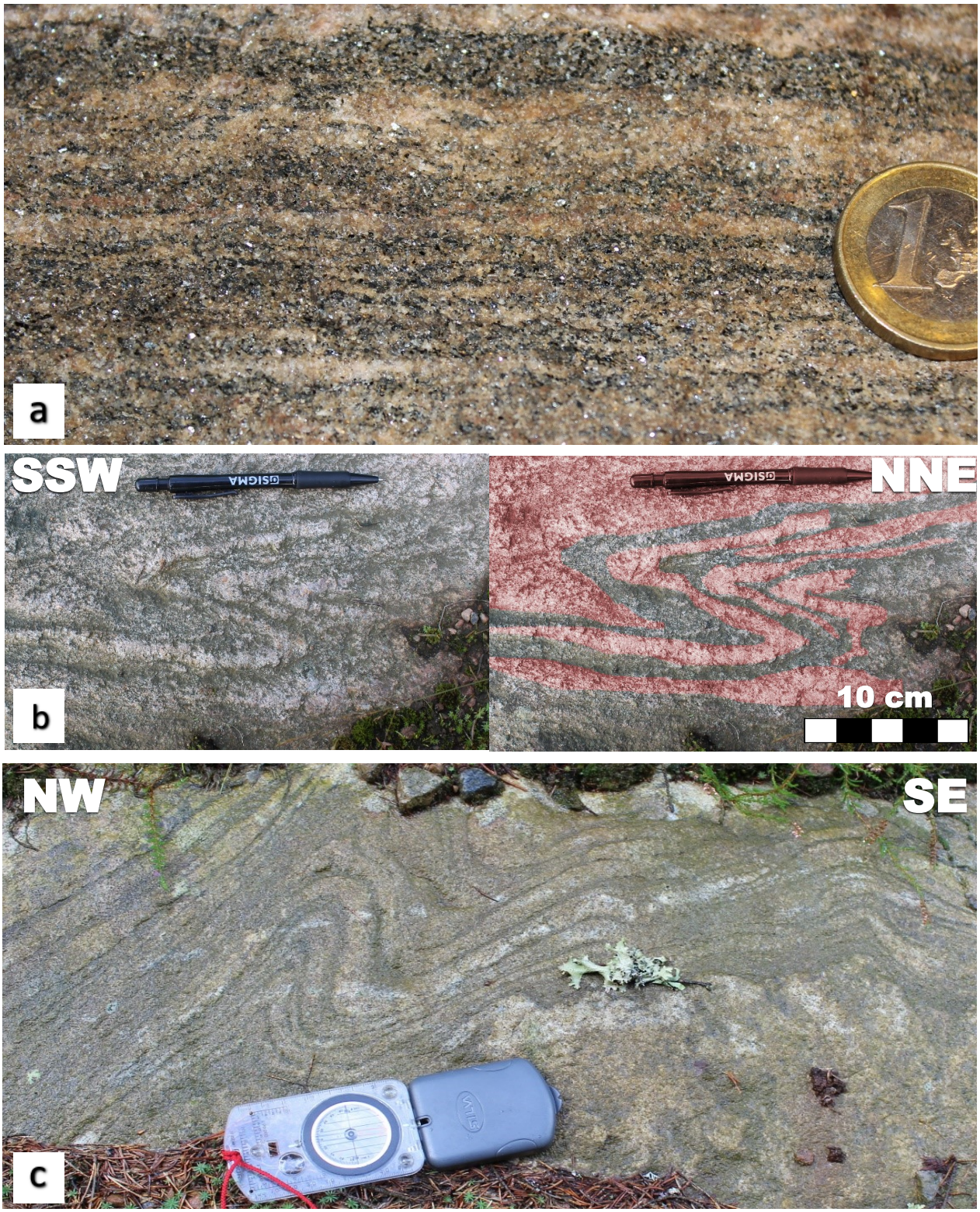

Fig. 9. Examples of migmatitic orthogneisses. (a) Thinly banded granitic gneiss from south of Oxås. Dark-colored bands are rich in biotite, whereas lighter ones are rich in quartz, plagioclase and K-feldspar. (b) Tight recumbent fold in migmatitic granitic gneiss at Fållen (BRO17080B; surface dipping gently towards the south; in the right figure leucosome is colored red for clarity). The fold axial plane is SSW-dipping. (c) Folded stromatic layering in pinkish granitic migmatite gneiss. Sub-horizontal outcrop north of Stenbrohult (BRO17025), with compass, 17 cm long, for scale. The fold axial plane is NE-dipping.

is composed of whiteish plagioclase grains, pinkish K-feldspar and translucent quartz grains. The pegmatitic dykes, with widths of up to 0.2 meters, crosscut not only the gneissic foliation, but notably also the macroscopic folds. Lastly, at Stenbrohult (BRO17022), an earlier generation of pegmatitic veins

Fig. 10. Examples of migmatitic orthogneisses and leucocratic granitic gneiss. (a) Stromatic migmatitic orthogneiss at Östra Kalvia (BRO17083) with leucosome veins composed of plagioclase, K-feldspar and quartz. The leucocratic leucosome veins have dark-colored mafic selvedges. (b) Close-up of the mafic selvedge in the same outcrop as (a). The patch at the lower right of the hammer shows a less altered surface of the rock. (c) Medium grained leucocratic granitic gneiss occurring within the migmatitic garnet amphibolite at Lalåsen (BRO170035).

within the migmatitic orthogneiss show ptygmatic folding and boudinage (Fig. 11c).

4.4.2 Microtextures – polarized microscopy

The rocks in the investigated area are analogous to studied thin sections from five localities: Ma, Nennesholm, NE. Broaryd and SW. Smålandsstenar (JAN040001A, JAN040015A, JAN040074A and JAN040181A; Appendix III). The rocks are fine- to medium grained with abundant plagioclase, quartz and a varying K-feldspar content. In the sample from Ma (JAN040001A) 200 µm thick quartz ribbons are located near plagioclase, microcline and small grains of titanite and ilmenite (Fig. 12a). The gneissic foliation in this sample is defined by quartz ribbons and elongated mafic minerals, such as biotite and hornblende (Fig. 12b). This gneissic metagranite is found less than 5 km north east of the studied area.

Some larger plagioclase grains (variably sericitized) have small inclusions (Fig. 12c) of biotite, plagioclase, hornblende and opaques (Fig. 12d). The rock types are generally uneven grained and these larger plagioclase grains are consequently not megacrysts. The K-feldspar rich varieties are better represented at

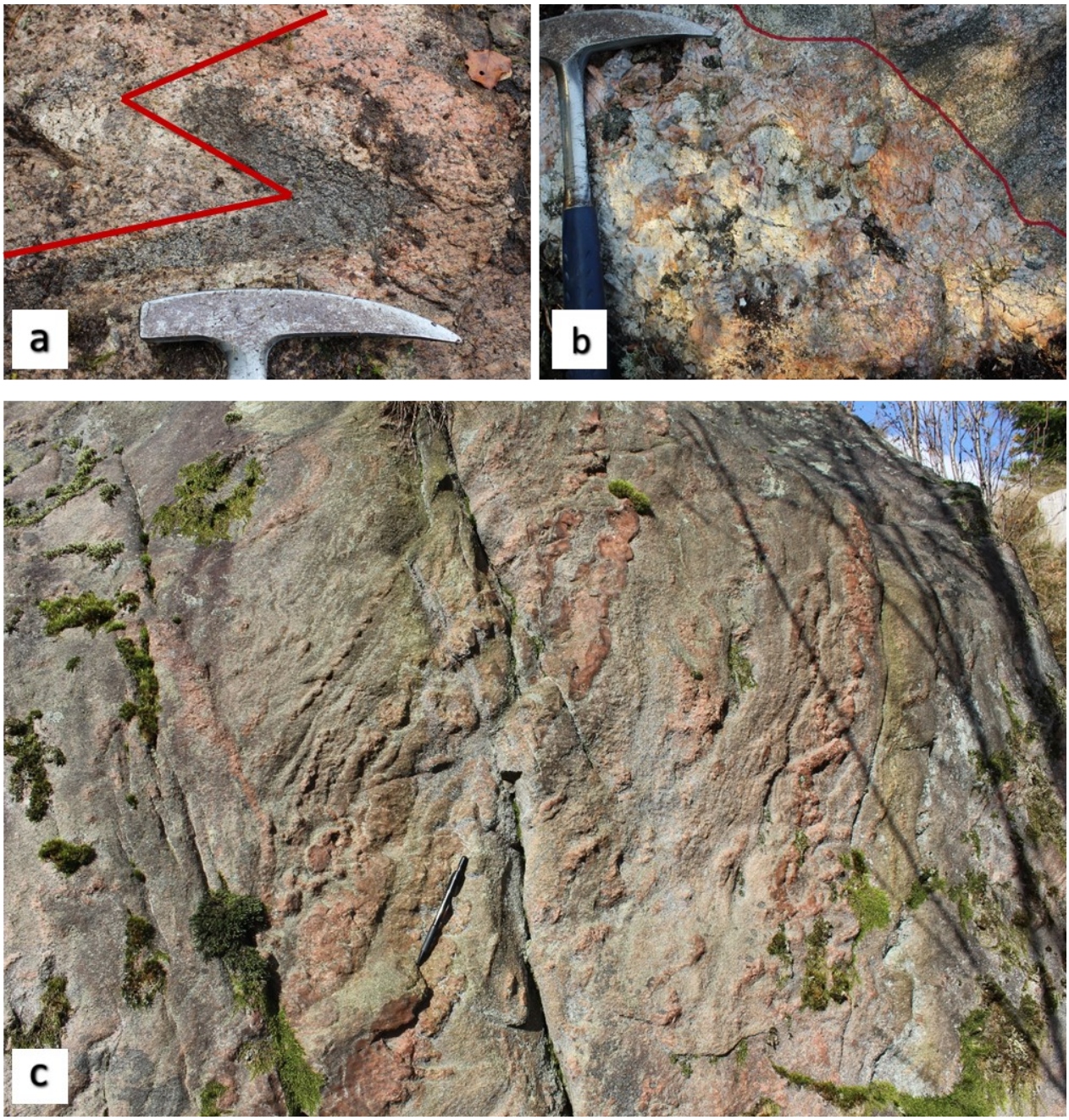

Fig. 11. Examples of migmatitic gneisses. (a) Small-scale fold in migmatitic gneiss south of Oxås (BRO17088; red lines mark fold). (b) Crosscutting, undeformed pegmatite dyke (lower left), composed of cm-sized crystals of quartz, K-feldspar and plagioclase, in quartz-feldspar rich migmatitic orthogneiss (right) at Pellabo (BRO17103). The red line indicates the contact between the dyke and the host rock. (c) Ptygmatic folds of pinkish leucosome in migmatitic orthogneiss at Stenbrohult (BRO17022). At the lower center of the image is a pen (14 cm) for scale.

Nennesholm (JAN040015A) as this sample have large domains composed almost exclusively of microcline (Fig. 12e). This sample is taken from an outcrop located 15 km north east of the area and used to represent the K-feldspar rich variety present within the mapped area. Samples with a weaker gneissic banding is also present in the vicinity. At SW. Smålandsstenar (JAN0181A), approximately 3 km east of Samserydssjön, the rock has a tonalitic-granodioritic composition with a weak gneissic banding represented by elongated hornblende grains (Fig. 12f). The sample is poor in K-feldspars and contains minor biotite, iron oxides and ilmenite.

4.5 Coronitic metagabbro

Coronitic metagabbro occurs just north of Bassö, in the central parts of the mapped area. The main outcrop is located at the southern edge of a hill north of Bassö

Fig. 12. Microphotographs (XPL) of different migmatitic metagranites and gneisses. (a) Metagranite from Ma (JAN040001A). Elongated coarse quartz ribbon with surrounding twinned plagioclase and minor hornblende (brown). (b) The same sample as in (a) showing plagioclase, microcline, elongated thin hornblende and biotite grains, together with fewer small subrounded unidentified accessory mineral grains (light blue), possibly magmatic zircon. The foliation is defined by the mafic minerals and the felsic mineral domains throughout the sample. (c) Large anhedral twinned plagioclase grain in metagranite from Ma (JAN040001A). (d) Migmatitic orthogneiss, with uneven-grained texture composed of plagioclase, quartz, and microcline, from Broaryd (JAN040074A). (e) Photomicrographs of a K-feldspar rich migmatitic metagranite at Nennesholm (JAN040015A). The image shows microcline (Kfs) with tartan twinning and uneven grain size. (f) Sample from SW. Smålandsstenar (JAN040181A) presenting a plagioclase and quartz rich rock with a weak gneissic foliation composed of elongated hornblende grains.

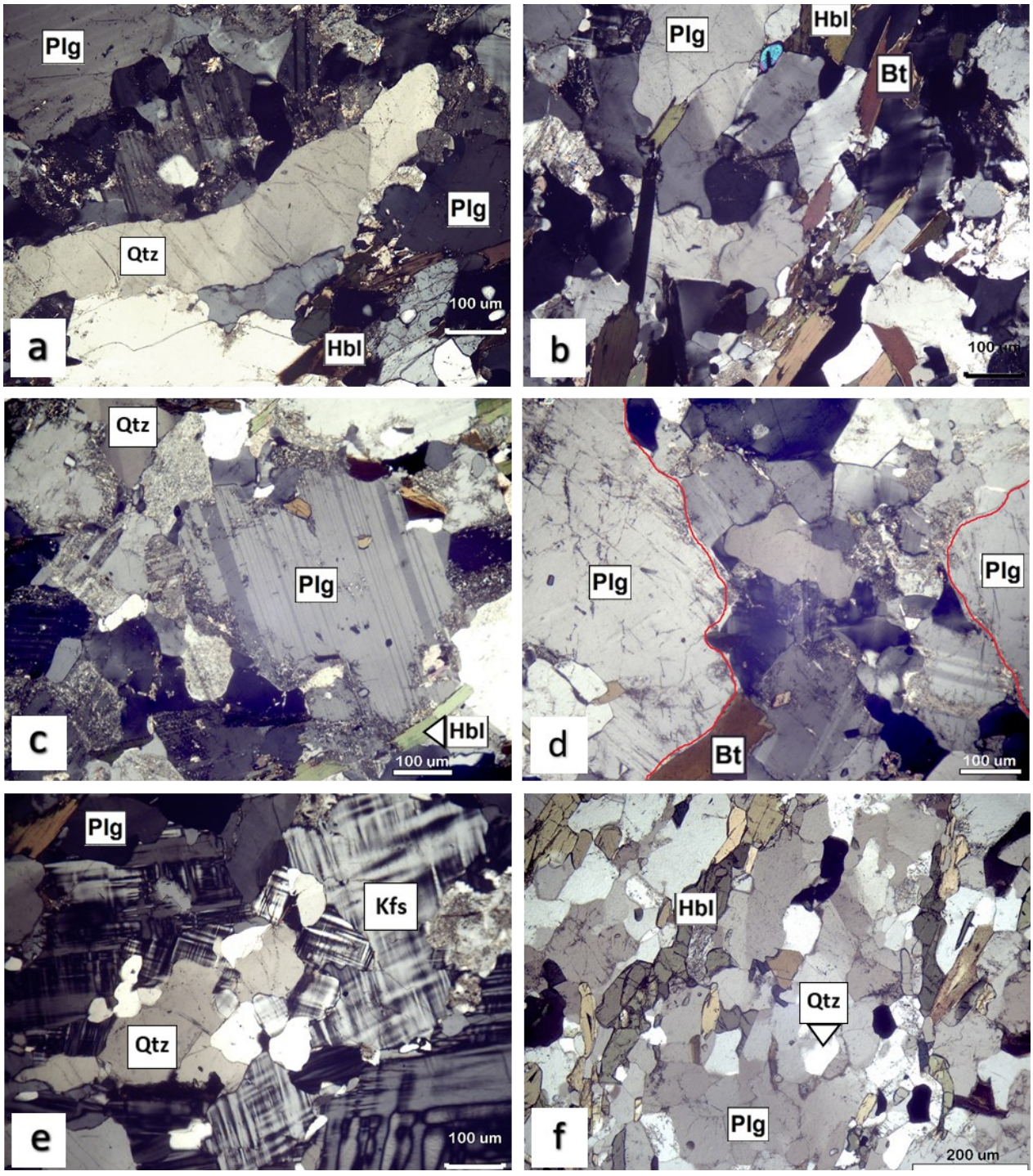

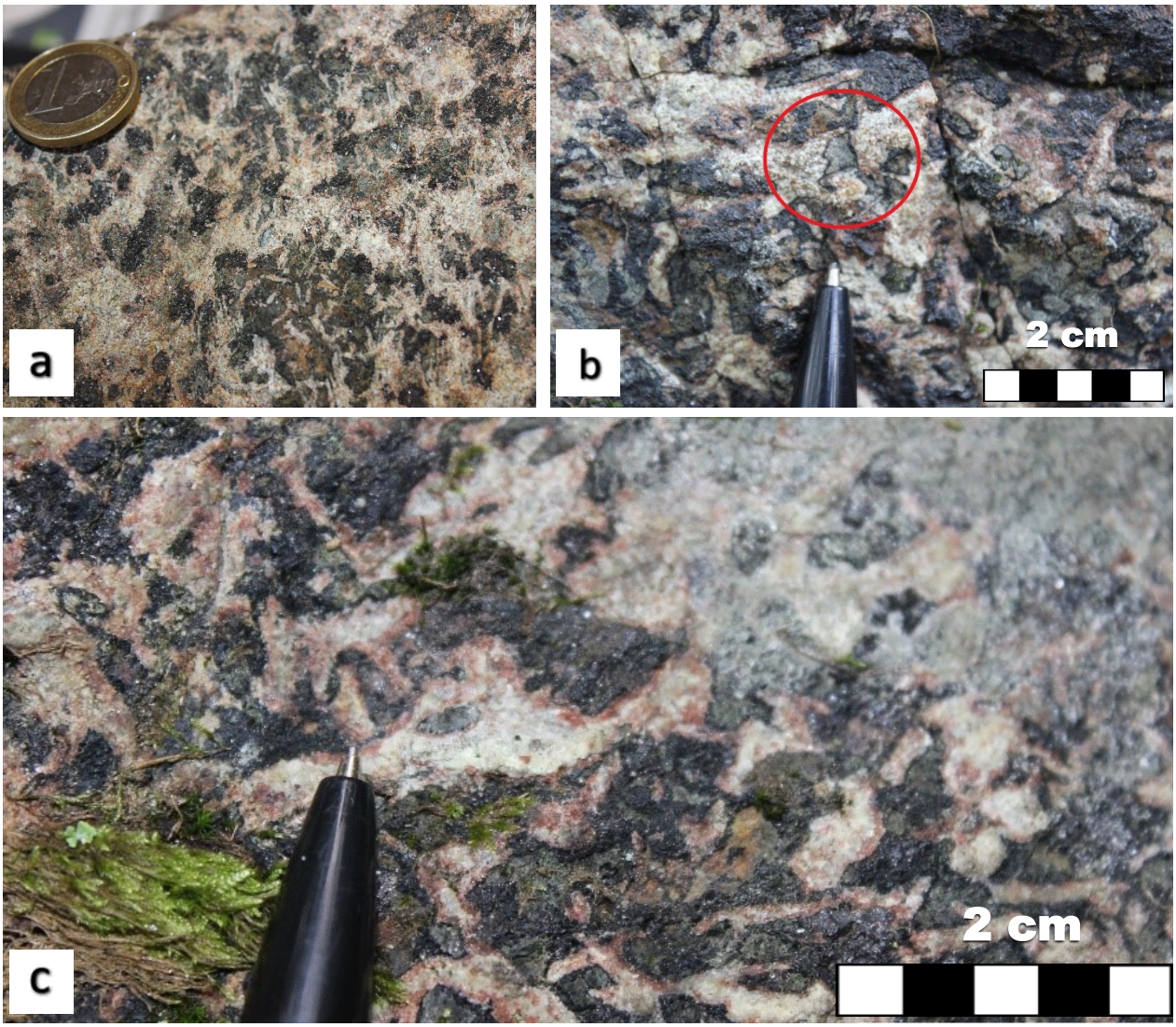

Fig. 13. Coronitic metagabbro at Bassö (BRO17075). (a) Within the mafic domains, elongated light-colored laths are easily distinguished. These are relict igneous plagioclase grains, composed of aggregates of metamorphic plagioclase. (b) Dark-colored corona of amphibole around a clinopyroxene grain (pale green). (c) Velvet-red coronas of garnet around mafic aggregates of amphibole, pyroxene and biotite. The light-colored domains are composed mostly of plagioclase.

(BRO17075A and BRO17075B). Other outcrops at the peak of the Bassö hill (BRO17091 and BRO17092) consisting of the same rock type, implies that the entire hill is composed of coronitic metagabbro.

4.5.1 Macroscopic description

The coronitic metagabbro is a relict coarse grained gabbro, partly recrystallized into fine grained metamorphic minerals. Remnant pyroxene grains are surrounded by coronas of amphibole, or double coronas of amphibole and velvet-red garnet. Double corona is the formation of two coronas in between the same minerals. Plagioclase forms elongated laths and also fine grained aggregates that surrounds the mafic minerals. The pseudomorphed plagioclase domains (whiteish), located in mafic aggregates, keep an igneous lath shape (Fig. 13a). Dark green domains are composed mainly of clinopyroxene and rimmed by blackish amphibole (Fig. 13b). Velvet-red minute garnet grains surround the dark minerals, forming a coronitic texture (Fig. 13c). Light colored domains are composed mainly of plagioclase, with minor quartz.

4.5.2 Microtextures – polarized microscopy and SEM

The coronitic texture is apparent in thin sections. Double coronas of garnet and hornblende are located between plagioclase and clinopyroxene grains (Fig. 14a). Both samples are from Bassö (B6 and JAN040075A; Appendix III). The garnet crystals are almost perfectly euhedral in contact with the plagioclase domains and contrastingly strongly anhedral with numerous inclusions towards the hornblende grains (Fig. 14b). In most of the rock amphibole has partially or completely replaced igneous pyroxene and in places being substituted by radiating idioblastic biotite aggregates (Fig. 14c). Such biotite aggregates are often associated with igneous FeTi-oxides. The

Fig. 14. Microphotographs (PPL) of coronitic metagabbro from Bassö (JAN040075A). (a) Double corona of garnet and hornblende (green) between plagioclase and clinopyroxene grains. The clinopyroxene grain has orthopyroxene lamellae forming a planar texture within the grain. (b) Corona of garnet around mafic aggregate composed of hornblende (green) and idioblastic biotite (brown). The garnet grains are euhedral next to the plagioclase and strongly anhedral next to hornblende. The biotite grains are elongated, lath shaped and oriented towards the garnet corona. (c) Corona of garnet around biotite aggregate (brown) with a small rim of hornblende (green).

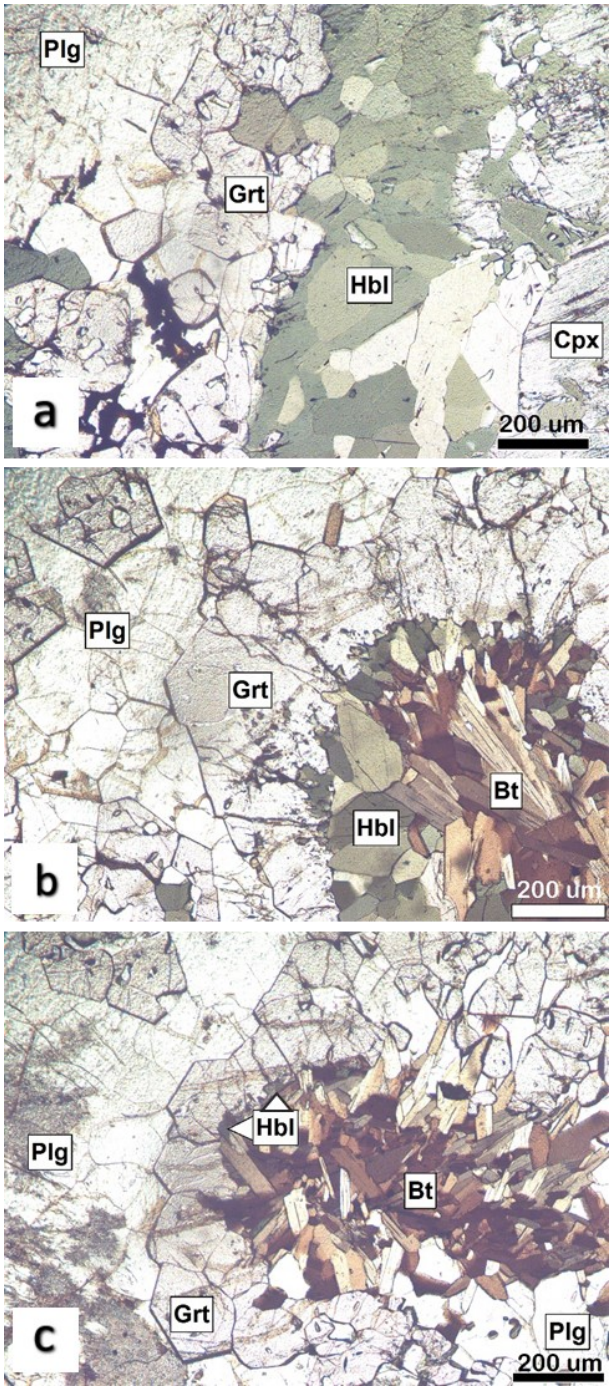

coronitic metagabbro also contains ilmenite, apatite, iron oxides, zircon, rutile and Fe-sulphide.

The rims of igneous plagioclase laths are in many places partially recrystallized/consumed. Fractures in pyroxene grains are filled with small hornblende grains (Fig. 15a). Within the same sample garnet coronas have formed around FeTi-oxide domains (Fig. 15b). Both biotite and hornblende are present in the vicinity to such domains. The igneous plagioclase laths are better seen in a scan of the thin section (Fig. 15c), where the coronitic texture is more evident.

Symplectite-like intergrowths of garnet and amphibole are frequent along the grain boundaries between garnet and granoblastic hornblende aggregates around (Fig. 16a). Zoned plagioclase grains are common within the coronitic metagabbro, especially at Bassö (VV14BRO1), these grains lack twinning and are partially or completely rimmed by double coronas of garnet and hornblende grains (Fig. 16b and c).

At Bassö (VV14BRO1) the cores of the plagioclase grains are dusty and the rims are clear. Clouded plagioclase is due to minute inclusions of iron and titanium oxides. There is a slight increase in anorthite from rim to core, with values varying from An11 at the rim to An25 at the core of the grain. The rim of the grain is in contact with a garnet corona (Fig. 16b and c). The plagioclase is present both on the inner and outer parts of the garnet corona, suggesting that these two minerals formed simultaneously. Hornblende has formed a partial corona alongside the garnet corona forming an incomplete double corona. The incomplete double corona has formed in between plagioclase and clinopyroxene grains, equally to previously mentioned double corona formations.

At Bassö (B6) garnet coronas around orthopyroxene grains are common. The core of the orthopyroxene grains represents a symplectite-like texture of ilmenite (light colored), orthopyroxene (light grey) and hornblende (dark grey) (Fig. 17a). The garnet is almanditic (Fe-rich) in composition, Alm64, whereas the plagioclase is anorthitic, An45 (Appendix V, Table V.II, Spectrum 1 and 2). Clinopyroxene wit-

Fig. 15. Coronitic metagabbro from Bassö (B6). (a) Elongate remnant of igneous clouded plagioclase lath partly consumed at the rims (XPL). The plagioclase lath is surrounded by large grains of remnant igneous clinopyroxene and partly rimmed by minute grains of hornblende (brown). (b) Garnet corona around a Fe-Ti oxide. Garnet has partly consumed the igneous plagioclase lath and formed euhedral crystal faces adjacent to plagioclase. On the other side of the corona, a symplectite-like texture appears between garnet, hornblende (green) and biotite (brown) (PPL). (c) Scan of thin section B6 from Bassö. The elongated plagioclase laths are clearly seen in this image. The main minerals are marked, clinopyroxene (light green), plagioclase (grey), hornblende (green), biotite (brown) and a garnet corona (colorless). Black colored areas represent opaques.

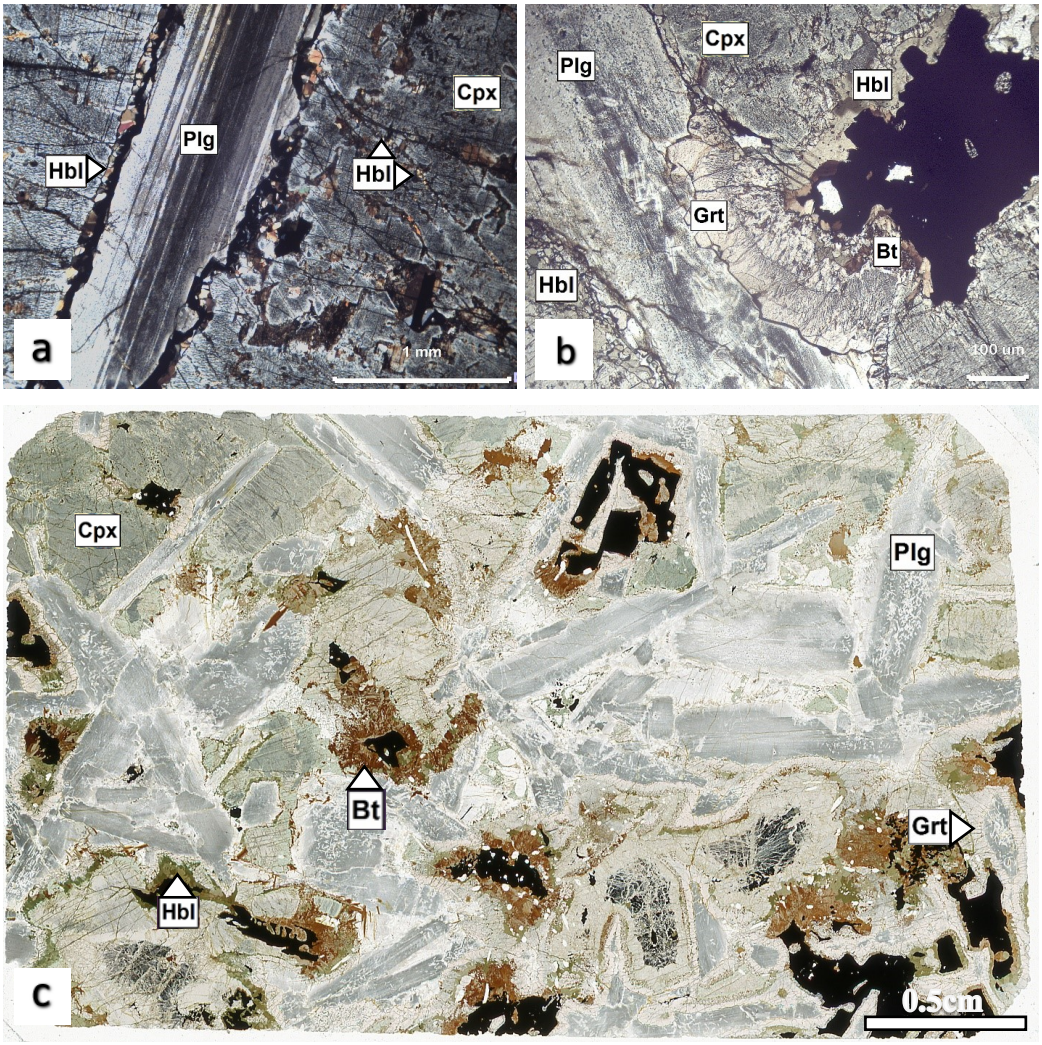

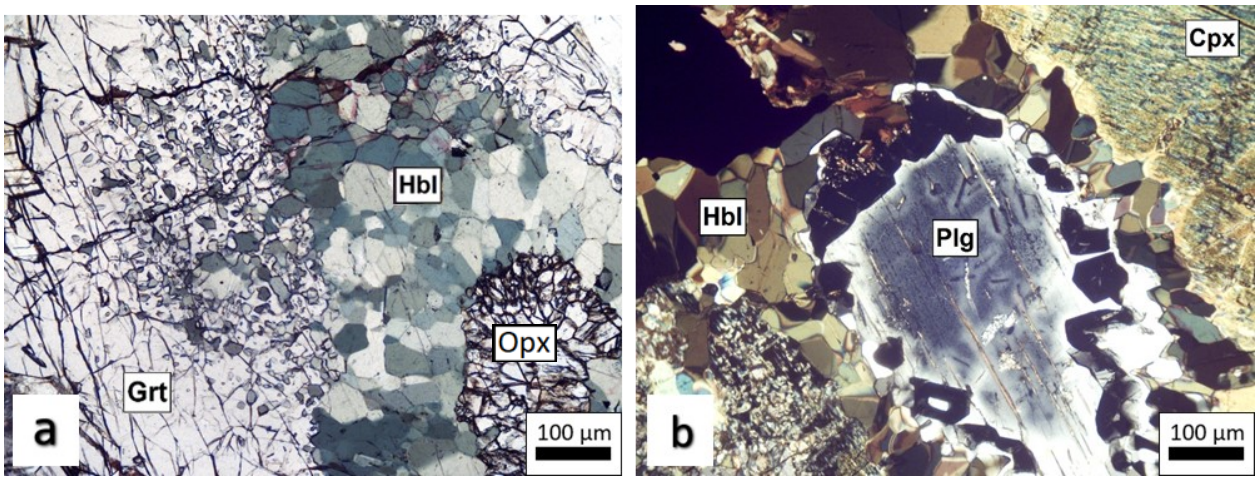

Fig. 16. Corona formations and small-scale symplectite-like microtextures in coronitic metagabbro at Bassö (VV14BRO1; XPL). (a) A symplectite-like reaction rim has formed between aggregated orthopyroxene grains and plagioclase (not featured) and is composed of garnet and hornblende (green). The hornblende forms an aggregate of small grains within the garnet grain. (b) Zoned plagioclase grain in coronitic metagabbro at Bassö (VV14BRO1). A double corona composed of garnet and hornblende surround the zoned plagioclase grain. The section features large clinopyroxene and hornblende grains.

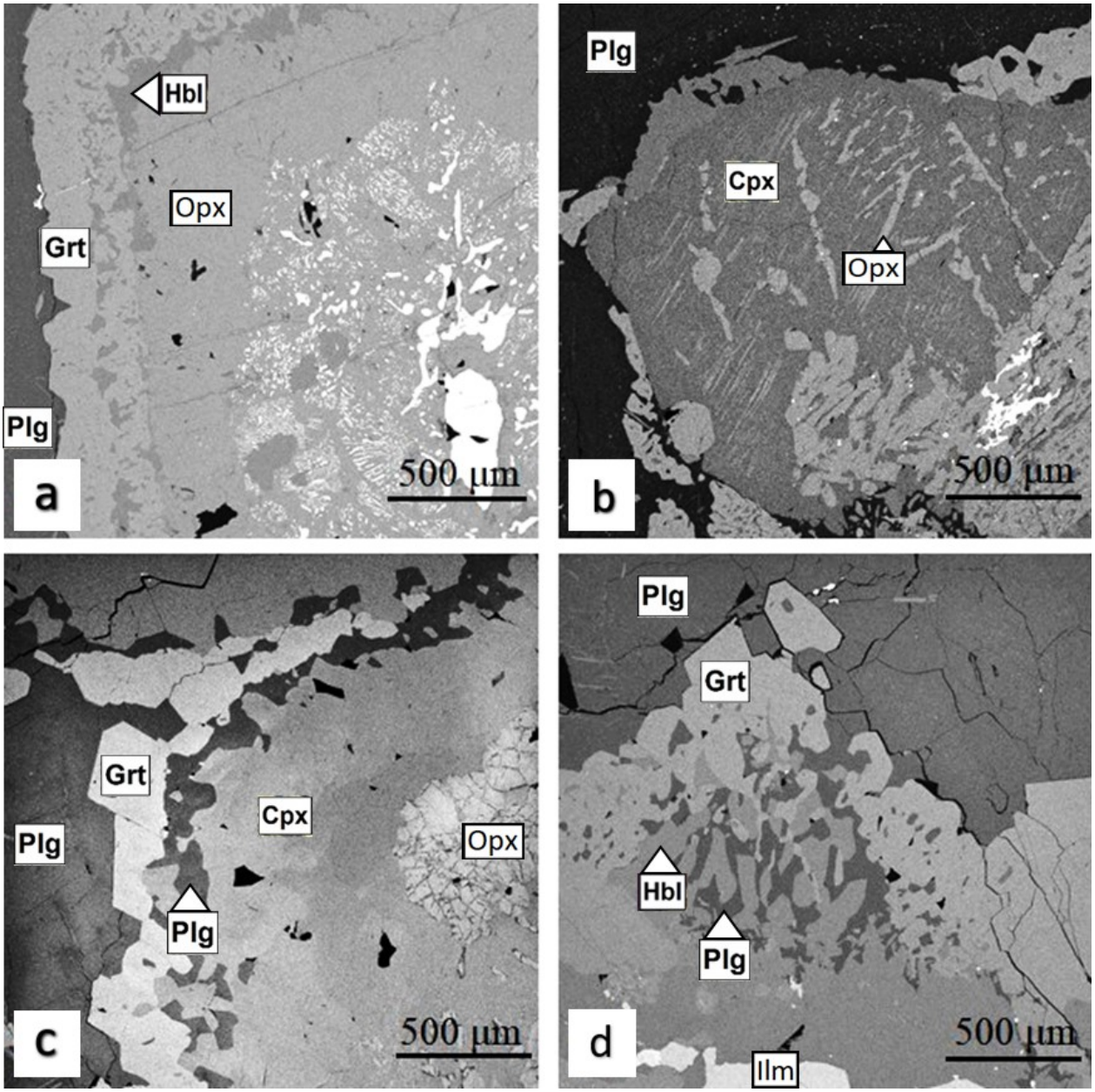

Fig. 17. Back-scattered electron images of coronitic metagabbro at Bassö (B6 and VV14BRO1). (a) Symplectitic texture in coronitic metagabbro at Bassö (B6). The sample presents a larger orthopyroxene grain with a garnet corona. The center of the grain has a symplectitic texture composed mainly of ilmenite and orthopyroxene. Minor hornblende is located between the garnet corona and the orthopyroxene grain. (b) Orthopyroxene lamellae in clinopyroxene grain at Bassö (B6). Minor inclusions in the grain are apatite and ilmenite. (c) Coronitic texture around clinopyroxene grain at Bassö (VV14BRO1). The garnet corona has formed between plagioclase and clinopyroxene. The center of the grain is composed of aggregates of orthopyroxene. (d) Corona of garnet at Bassö (VV14BRO1). The image presents a symplectite-like texture of garnet, plagioclase and hornblende. The center of the grain is completely replaced by ilmenite.

hin the thin section has the general formula $MgFeSi_2O_6$, corresponding to a clinopyroxene compositionally in between enstatite ($Mg_2Si_2O_6$) and ferrosilite ($Fe_2Si_2O_6$) (Appendix V, Table V.II, Spectrum 4).

Furthermore, at Bassö (B6) it is common for clinopyroxene grains to contain lamellae of orthopyroxene, together with minor inclusions of apatite, ilmenite and Fe-sulphide (Fig. 17b). The plagioclase adjacent to the pyroxene has a composition equal to An48 (Appendix V, Table V.III, Spectrum 57). Within the sample some grains of clinopyroxene has a peculiar core structure. The cores are composed of multiple subrounded orthopyroxene grains, together with varying amounts of opaques, such as FeTi-oxides (Fig. 17c). The sample from Bassö (VV14BRO1) has a so-called double corona formation between the clin-

opyroxene and the clouded plagioclase. In this case it is a garnet-hornblende corona, present within the entire sample. Accessory subrounded metamorphic zircon is nucleating at the rims of clinopyroxene grains.

Symplectite-like textures are also found at Bassö (VV14BRO1). An intergrowth of plagioclase (dark grey), hornblende (medium grey) and garnet (light grey) has formed between plagioclase and hornblende crystals (rims on igneous pyroxene; Fig. 17d). Locally, ilmenite (whiteish) and hornblende have replaced the former pyroxene grains completely.

5 Interpretations

The interpretations of the analyzed samples focus on the plausible monitors of recrystallization as well as evidence for high temperature and pressure metamorphism. The metamorphic grades within the Eastern Segment have recently been categorized based partly on metamorphic assemblages in an Fe-Ti-rich metagabbro, a protolith that can be traced throughout the Eastern Segment (Möller & Andersson, 2018). The presence or absence of hydrous fluids during metamorphism have a considerable impact on recrystallization. "Dry" rocks can preserve an igneous texture, as a lack of fluids limit the diffusion rate impeding recrystallization. Deformational differences can be caused by folding, the hinge zone of a fold can undergo both compression and extension depending on the type of fold and fluid percolation might be limited due to folding.

5.1 Migmatization

Different outcomes during metamorphism vary greatly depending on the chemical composition of the protolith and the presence of fluids (Sawyer, 2008). Migmatization is an indicator of high temperatures as partial melting of rocks require temperatures around 650 °C or higher, it also represent the peak of high-grade conditions reached in hydrated rocks. Contrarily, dehydrated rocks and restites are unable to form melts, hence they become dry and dehydrated granulite facies rocks under such conditions (Winter, 2014).

The coronitic metagabbro at Bassö (BRO17075; Fig. 13), is the only non migmatized sample, possibly due to the dry conditions within this complex. The coronitic metagabbro is characterized by a largely anhydrous mineral assemblage of orthopyroxene, clinopyroxene and plagioclase, together with minor hydrated ferromagnesian minerals, such as biotite and amphibole. The mineral assemblage that is characteristic of granulite facies and the overall "dry" rock conditions suggests that the coronitic metagabbro have been metamorphosed at granulite facies conditions, an indicator of high temperature and pressure. Minerals such as the plagioclase laths have recrystallized and are composed of aggregates of metamorphic plagioclase, likewise suggesting a high temperature conditions during metamorphism.

Elsewhere within the studied area migmatized samples dominate and migmatization is presented both in felsic and mafic rocks. At Vickelsbo (BRO17006B) the migmatitic garnet amphibolite is a mafic metatexite migmatite with two axial melt-filled weakness planes (Fig. 4c). These net structures of leucosome contain both mafic and felsic minerals similar to the host rock, an indicator that the melt originated in situ (Sawyer, 2008). The leucosome within the rock is therefore interpreted to be a segregated partial melt from the host rock. The foliation of the host rock is obscured by glacial alteration, although it can be assumed that the direction of foliation follows the slightly more consistent leucocratic veins (horizontally in Fig. 4c). Drainage of melt possibly caused minor veins and structures to merge together. A temperature interval is arduous to define based solely on migmatization, as more competent mafic rock may cause less melt than a gneissic protholith at the same temperature (Sawyer, 2008). The observed features are nevertheless indicative of high temperatures during metamorphism.

Contrarily, crosscutting pegmatitic dykes with a mineral assemblage of plagioclase, K-feldspar and quartz possibly have an external melt source. This is suggested as the chemical proportions of the components are more granitic, than would be expected from a melted amphibolite. Post-kinematic pegmatitic dykes within the Eastern Segment are common and have been dated to 0.96-0.93 Ga using U-Pb dating (Möller & Andersson, 2018). This age is similar to that of the syn-kinematic veins and dykes, dated to 0.96-0.95 Ga within the Eastern Segment (op cit.). The pegmatitic dykes do not present strained minerals and the intrusion hence likely occurred after the deformational event that deformed adjacent rocks. The numerous pegmatitic dykes within the study area have not underwent metamorphism and are better used in geochronology, although not a subject of this paper.

Lastly, the main ferromagnesian minerals within the migmatitic orthogneisses are biotite and hornblende (Fig. 12). Above-mentioned hydrous minerals and leucosome within the felsic rocks indicate presence of fluids during partial melting in the area. Different rock complexes within the study area have been subjected to uneven distribution of hydrous fluids, as both "dry" and "wet" rocks coexist. Possibly as deformation inhibited fluids from percolating freely within the metamorphosed area.

5.2 Recrystallization monitors

Elongate quartz ribbons in the migmatitic orthogneiss (Fig. 12a) is a high temperature microtexture. The quartz ribbons are composed of a few large grains that give evidence of high-temperature dynamic recrystallization followed by grain-boundary area reduction (Tual et al., 2015 and references therein).

Crystallization from a melt is demonstrated by a polygonal texture of quartz and feldspar grains where the boundaries meet in triple junctions with approximately 120° angles between the grains (Winter, 2014). The size of the polygonal grains is dependent on temperature and the type of fluids percolating within the system, where a higher temperature and aqueous fluids promote a coarser grain size (Winter, 2014). Mesosome patches in the migmatitic orthogneisses have a fine grained polygonal texture suggesting that the rock experienced high-grade metamorphic conditions and as the peak conditions where reached subsequent cooling was relatively fast.

Similarly, the analyzed migmatitic gneisses

have a medium to coarse grained gneissic fabric and previous structures have been almost completely annealed. Recrystallization of grains is promoted by increasing temperature, generally resulting in an increased grain size (Winter, 2014). Annealing of previous structure and the medium to coarse grain size therefore supports a high temperature metamorphism.

Evidence of retrograde reactions include the presence of microcline within migmatitic orthogneisses. During retrograde reactions orthoclase commonly recrystallizes into the low-temperature K-feldspar microcline that is stable at temperatures below 500 °C (Haldar & Tišljar, 2013). This is noted in the migmatitic orthogneiss within abundant microcline presenting the typical albite and pericline twinning (Fig. 12e).

5.3 Microtextures

Reaction rims form in different metamorphic settings both in response to prograde and retrograde metamorphic reactions. The limited access to aqueous fluids inhibits the diffusion of chemical components and unable equilibrium conditions to be reached. Coronas or reaction rims are local isolated replacement features along grain boundaries (Passchier & Trouw, 2005). Coronas surround a mineral and form as adjoint minerals react and as diffusion of chemical components is low during a series of metamorphic reactions (Hollocher, 2014).

The most common reaction rims within the study area are seen in the coronitic metagabbro at Bassö, with garnet coronas around pyroxenes (Fig. 13). As the coronitic metagabbro is not migmatized nor annealed, the prominent coronitic texture suggests solid-state reactions in high-grade dry rock conditions. The slow cooling of these rocks permits retrograde reactions and the reactions do not readily run to completion as there is lack of fluids to diffuse the chemical components (Winter, 2014). Garnet coronas often form in between plagioclase and mafic minerals, as garnet require both aluminum and iron to crystallize. Aluminum is taken from the plagioclase and iron from the mafic mineral. Other metamorphic ferromagnesian minerals are usually formed in the process, such as biotite, hornblende and metamorphic pyroxene (Winter, 2014). The occurrence of a double corona at Bassö (Fig. 14a) is interpreted to have formed during retrograde reactions. Retrograde reactions between pyroxene and plagioclase cause the formation of both garnet, hornblende and biotite (Fig. 14b and c). Likewise, the resorbed garnet grains with numerous hornblende inclusions and a symplectite-like texture likely formed in the same process (Fig. 14b and 16a). The crystal faces of biotite are idioblastic and oriented parallel causing a low angle boundary between the grains, requiring minimal energy during formation.

Other features, for instance, orthopyroxene lamellae within clinopyroxene grains at Bassö (Fig. 14a), are interpreted to have formed as a result of an exsolution reaction during cooling of the metagabbroic rock. Pyroxenes have wider fields of solid solutions at higher temperatures, as temperature decrease the composition is adjusted in the solid state by exsolving a separate phase (Winter, 2014). In this case producing parallel lamellae intergrowths of orthopyroxene within the host clinopyroxene grain. It is indicative of high temperatures during metamorphism. Recrystallized aggregates of orthopyroxene at W. Broaryd, on the other hand, are suggested to have formed from magmatic olivine grains present in the gabbroic protholith (Fig. 16a and 17c).

5.4 Protholiths and origin of the rocks

An igneous origin of a rock can be determined from remnant igneous minerals and several parameters can be stabilized to interpret the origin of a mineral. The shape and size of a mineral can give indications on the origin. It is known that elongate euhedral plagioclase laths suggest an igneous origin (Vernon, 2004). At Bassö (B6 and VV14BRO1) relict igneous features such as elongated plagioclase laths together with partly preserved igneous clinopyroxene reveals the phenocryst texture of the protholith (Fig. 15c). A gabbro is an igneous rock composed mainly of plagioclase and pyroxene, it may also contain smaller amounts of olivine, biotite and amphibole (Vernon, 2004). The rock is consequently interpreted as a metagabbroic rock with a relict igneous texture.

A relict texture is a reaction texture that is dominantly preserved in less deformed rocks, and not directly correlated to a specific metamorphic grade. The geological bedrock map indicates that Bassö is located in the hinge zone of a regional scale fold. The fold zone, or hinge zone, may be slightly less affected by deformation than the limbs of the fold. Possibly causing a less homogeneous deformation in the area and preventing fluids from entering the rock system. The locality Bassö (BRO17075) composed of coronitic metagabbro is interpreted to be located in a less deformed section of the rock complex, due to the position of the rock complex within the fold.

The effects of fluids during metamorphism is known to have a significant effect (Winter, 2014). It may therefore also be suggested that the migmatitic amphibolite and the coronitic metagabbro in question have the same protholith. Recent research of metamorphic grades within the Eastern Segment, based on metamorphic assemblages in a Fe-Ti rich metagabbro traceable throughout the Eastern Segment further supports this (Möller & Andersson, 2018). Local lack of fluids may therefore explain why the coronitic metagabbro preserved a relict texture and is the only non migmatized sample within the studied area.

6 Suggestions for further studies

- Sample garnet porphyroblasts from migmatitic garnet amphibolites in the nearby area to see if there is any zoning.
- Study regional scale folds affecting the migmatized amphibolite and the coronitic metagabbro within the Eastern Segment. Analyze if there is a general difference in deformation between the hinge zone and the limbs of the folds and if it can be related to lack of penetration of fluids during metamorphism.

7 Conclusions

- Strongly migmatized garnet amphibolites and

orthogneisses within the studied area of the Eastern Segment suggests temperatures above 650 °C during metamorphism. A high temperature during metamorphism is furthermore confirmed by quartz ribbons, annealing of previous structures and a coarse grained fabric in migmatitic orthogneisses.

- Pervading coronitic texture in metagabbroic rocks is an indicator of high-grade metamorphism in dry conditions, reaching granulite facies. The mineral assemblage is characteristic for granulite facies and the relict igneous texture of the rock confirms the dry conditions, as fluids did not percolate the system and reactions did not run to completion. Resulting in a heterogeneously metamorphosed section of the metagabbroic rock.
- The mafic bedrock within the area is interpreted to have a similar protholith. The fact that the coronitic metagabbro at Bassö is located in the hinge zone of a fold and that the surrounding migmatitic amphibolite is located along the limbs of a fold is interpreted to cause notable difference during metamorphic deformation due to both lack of percolating fluids and deformational differences within the fold.

8 Acknowledgements

A special thanks to my Supervisor Charlotte Möller at Lund University for suggesting me this field-based mapping project and for all her help and corrections made to improve my work. I am also grateful for the help I got from Jenny Andersson at SGU and for the thin sections she provided.

Thanks to Victoria Beckman at Lund University who provided me with valuable thin sections for this project. Thanks to the dear owners of Sotanäs Bed&Breakfast at lake Fegen in Halland for their encouragement during all those rainy days and for accommodating me during my field work.

A sincere thank you to all my fellow students at Geocentrum, Lund University, for constant support and optimism during this entire project.

9 References

Andersson, J., Söderlund, U., Johansson, L. & Möller, C., 1999. Sveconorwegian (-Grenvillian) deformation, metamorphism and leucosome formation in SW Sweden, SW Baltic Shield: constraints from a Mesoproterozoic granite intrusion. Precambrian Research, 98, 151-171.

Andersson, J., Möller, C., & Johansson, L. (2002). Zircon chronology of migmatite gneisses along the Mylonite Zone (S. Sweden): a major Sveconorwegian terrane boundary in the Baltic Shield. Precambrian Research, 114, 121–147.

Bingen, B., Davis, W., Hamilton, M., Engvik, A., Stein, H.J., Skår, Ø., & Nordgulen, Ø., 2008. Geochronology of high-grade metamorphism in the Sveconorwegian belt, S Norway: U–Pb, Th–Pb and Re–Os data. Norwegian Journal of Geology, 88, 13-42.

Bingen, B., Skår, Ø., Marker, M., Sigmond, E.M.O., Nordgulen, Ø., Ragnhildstveit, J., Mansfeld, J., Tucker, R.D. R. & Liègeois, J.P., 2005. Timing of continental building in the Sveconorwegian orogen, SW Scandinavia. Norwegian Journal of Geology, 85, 87-116.

Brander, L., Appelquist, K., Cornell, D. & Andersson, U., 2012. Igneous and metamorphic geochronologic evolution of granitoids in the central Eastern Segment, southern Sweden. Int. Geo. Rev., 54(5), 509-546.

Christoffel, C., Connelly, J. & Åhäll, K., 1999. Timing and characterization of recurrent pre-Sveconorwegian metamorphism and deformation in the Varberg–Halmstad region of SW Sweden. Precambrian Research, 98, 173-195.

Connelly, J. N., Berglund, J. & Larson, S. Å., 1996. Thermotectonic evolution of the Eastern Segment. Brewer, T. S. (ed.), Precambrian Crustal Evolution in the North Atlantic Region, Geological Society Special Publication, 112, 297-313.

Haldar, S. & Tišljar, J., 2013. Introduction to Mineralogy and Petrology. Elsevier, pp. 354.

Hansen, E., Johansson, L., Andersson, J., LaBarge, L., Harlov, D., Möller, C., & Vincent, S. (2015). Partial melting in amphibolites in a deep section of the Sveconorwegian Orogen, SW Sweden. Lithos, 236, 27–45.

Hegardt, A.E., Cornell, D.H., Claesson, L., Simakov, S., Stein, H.J., & Hannah, J.L., 2005. Eclogites in the central part of the Sveconorwegian, Eastern Segment of the Baltic Shield: support for an extensive eclogite terrane. GFF, 127, 221-232.

Hollocher, K., 2014. A Pictorial Guide to Metamorphic Rocks in the Field. Taylor & Francis Group, London, UK, pp. 310.

Hubbard, F., 1975. The Precambrian crystalline complex of south-western Sweden. The geology and petrogenetic development of the Varberg region. GFF, 97.3, 223-236.

Högdahl, K., Andersson, U.B., Eklund, O. (Eds.), 2004. The Transscandinavian Igneous Belt (TIB) in Sweden: A Review of Its Character and Evolution. Geological Survey of Finland Special Paper, 37, pp. 125.

Johansson, L. & Kullerud, L., 1993. Late Sveconorwegian metamorphism and deformation in southwestern Sweden. Precambrian research, 64, 347-360.

Johansson, L., Lindh, A., & Möller, C., 1991. Late Sveconorwegian (Grenville) high-pressure granulite facies metamorphism in southwest Sweden. Journal of Metamorphic Geology, 9, 283–292.

Kretz, R., 1983. Symbols for rock-forming minerals. Am. Mineral., 68, 277 - 279.

Li, Z.X., Bogdanova, S.V., Collins, A.S., Davidson, A., De Waele, B., Ernst, R.E., Fitzsimons, I.C.W., Fuck, R.A., Gladkochub, D.P., Jacobs, J., Karlström, K.E., Lu, S., Natapov, L.M., Pease, V., Pisarevsky, S.A., Thrane, K. & Vernikovsky, V., 2008. Assembly, configuration, and break-up history of Rodinia: A synthesis. Precambrian Research, 160, 179-210.

London, D., 2008. Pegmatites. The Canadian Mineralogist, Special Publication 10, pp. 347.

Möller, C. & Andersson, J., 2018. Metamorphic zoning and behaviour of an underthrusting continental plate. Journal of Metamorphic geology, 36, 567-589.

Möller, C., 1998. Decompressed eclogites in the Sveconorwegian(–Grenvillian) orogen of SW Sweden: petrology and tectonic implications. Journal of Metamorphic geology, 16, 564-656.

Möller, C., 1999. Sapphirine in SW Sweden: a record of Sveconorwegian(–Grenvillian) late-orogenic tectonic exhumation. Journal of Metamorphic Geology, 17, 127-141.

Möller, C., Andersson, J., Lundqvist, I. & Hellström, F., 2007. Linking deformation, migmatite formation and zircon U–Pb geochronology in polymetamorphic orthogneisses, Sveco-norwegian Province, Sweden. Journal of Metamorphic Geology, 25, 727-775.

Möller, C., Andersson, J., Brendan, D. & Lundin, I.A., 2015. Exhumation of an eclogite terrane as a hot migmatitic nappe, Sveconorwegian orogen. Lithos, 226, 147-168.

Möller, C., Bingen, B., Andersson, J., Stephens, M.B., Viola, G. & Scherstén, A., 2013. Comment: A non-collisional, accretionary Sveconorwegian orogen - Comment. Terra Nova, 25, 165-168.

Nolte, N., Kleinhanns, I. C., Baero, W., & Hansen, B. T., 2011. Petrography and whole-rock geochemical characteristics of Västervik granitoids to syenitoids, southeast Sweden: constraints on petrogenesis and tectonic setting at the southern margin of the Svecofennian domain. GFF, 133, 173–196.

Passchier, C.W. & Trouw, R.A.J., 2005. Microtectonics. Springer Science & Business media, pp. 366.

Petersson, A., Scherstén, A., Andersson, J. & Möller, C., 2013. Zircon U–Pb and Hf – isotopes from the eastern part of the Sveconorwegian Orogen, SW Sweden: implications for the growth of Fennoscandia. Geological Society of London Special Publications, 389, 281-303.

Pinan-Llamas, A., Andersson, J., Möller, C., Johansson, L. & Hansen, E., 2015. Polyphasal foreland-vergent deformation in a deep section of the 1 Ga Sveconorwegian orogen. Precambrian research, 265, 121-149.

Sawyer, E.W., 2008. Atlas of migmatites. The Canadian mineralogist, Special Publication 9, NRC Research Press, Ottawa, Ontario, Canada, pp. 371.

Slagstad, T., Roberts, N.M.W., Marker, M., Røhr, T.S. & Schiellerup, H., 2013. A non-collisional, accretionary Sveconorwegian orogen. Terra Nova, 00(0), 1-8.

Stephens, M.B, & Andersson, J., 2015. Migmatization related to mafic underplating and intra- or back-arc spreading above a subduction boundary in a 2.0–1.8 Ga accretionary orogen, Sweden. Precambrian research, 264, 235-257.

Söderlund, U., Persson, P.O., Jarl, L.G., Stephens, M. & Wahlgren, C.H., 1999. Protolith ages and timing of deformation in the eastern, marginal part of the Sveconorwegian orogen, southwestern Sweden. Precambrian research, 94, 29-48.

Söderlund, U., Hellström, F. & Kamo, S., 2008. Geochronology of high-pressure mafic granulite dykes in SW Sweden; tracking the P-T-t path of metamorphism using Hf isotopes in zircon and baddeleyite. Journal of Metamorphic Geology, 5, 539-560.

Söderlund, U., Isachsen, C.E., Bylund, G., Heaman, L.M., Patchett, P.J., Vervoort, J.D. & Andersson, U.B., 2005. U-Pb baddeleyite ages and Hf, Nd isotope chemistry constraining repeated mafic magmatism in the Fennoscandian Shield from 1.6 to 0.9 Ga. Mineralogy and Petrology, 2, 174-194.

Söderlund, U., Möller, C., Andersson, J., Johansson, L. & Whitehouse, M.J., 2002. Zircon geochronology in polymetamorphic gneisses in the Sveconorwegian orogen, SW Sweden: ion microprobe evidence for 1.46–1.42 Ga and 0.98–0.96 Ga reworking. Precambrian Research, 113, 193-225.

Tual, L., Pinan-Llamas, A. & Möller, C., 2015. High-temperature deformation in the basal shear zone of an eclogite-bearing fold nappe, Sveconorwegian orogen, Sweden. Precambrian Research, 265, 104-120.

Tual, L., Pitra, P. & Möller, C., 2017. P–T evolution of Precambrian eclogite in the Sveconorwegian orogen, SW Sweden. Journal of Metamorphic geology, 35, 493-515.

Ulmius, J., Andersson, J., & Möller, C., 2015. Hallandian high temperature metamorphism at 1.45 Ga in continent Baltica: P–T evolution and SIMS U–Pb zircon ages of aluminous gneisses, SW Sweden. Precambrian Research, 265, 10–39.

Vernon, R.H., 2004. A Practical Guide to Rock Microstructure. Cambridge University Press, pp. 594.

Wang, X.D., & Lindh, A., 1996. Temperature–pressure investigation of the southern part of the Southwest Swedish Granulite Region. European Journal of Mineralogy, 8, 51–67.

Wik, N.-G., Andersson, J., Bergström, U., Claeson, D., Juhojuntti, N., Kero, L., Lundqvist, L., Möller, C., Sukotjo, S. & Wikman, H., 2007. Bedrock map Jönköping country, scale 1:250,000. Sveriges Geologiska Undersökning (SGU), K 61.

Winter, J.D. 2014. Principles of Igneous and Metamorphic Petrology. Pearson, pp. 738.

Appendix

I. Complete list of localities.
II. Map over the most important localities.
III. Thin section data.
IV. Aeromagnetic anomaly map from the geological survey of Sweden (SGU) over the study area.
V. Composition tables with mineral formula recalculation.

Appendix I.
Complete list of localities

I.I Complete list of localities with migmatitic garnet and garnet-poor amphibolites.

Migmatitic garnet and garnet-poor amphibolites						
Locality ID	Locality	Outcrops	Con-tact	SWEREF99TM N	SWEREF99TM E	Rock type
BRO17006B	Vickelsbo	B	X	6337929	0393164	Garnet amphibolite
BRO17008	Lalåsen			6337784	0394249	Garnet amphibolite
BRO17010	Lalåsen			6337728	0394340	Garnet amphibolite
BRO17011B	Lalåsen	B	X	6337677	0394493	Garnet amphibolite
BRO17017	Ramlareber-get			6338184	0394945	Garnet amphibolite
BRO17020	N. Stenbro-hult			6338113	0395391	Amphibolite, veins
BRO17022B	Stenbrohult	B	X	6337239	0395406	Garnet amphibolite
BRO17027	Ekedal			6337138	0394739	Garnet amphibolite
BRO17031	Åsenhöga			633----	039----	Garnet amphibolite
BRO17044	Prippebo			6335937	0394194	Garnet amphibolite
BRO17051	Kalvia			6336036	0393132	Garnet amphibolite
BRO17064A	V. Hyggås	A	X	6335885	0393583	Garnet amphibolite
BRO17068	Prippebo	A	X			
BRO17070	N. Bröttjaryd			6335296	0393708	Garnet amphibolite, veins
BRO17071B	N. Bröttjaryd	B	X	6334979	0393510	Garnet amphibolite
BRO17077	Toppen			633----	039----	Garnet amphibolite
BRO17080B	Fållen	B	X	6335413	0394127	Amphibolite, veins
BRO17081B	Älgabo	B		6333592	0396682	Garnet amphibolite
BRO170XX	N. Kalvia			6336017	0392875	Garnet amphibolite
BRO170XX	Ekedal			6336960	0394939	Garnet amphibolite
BRO17104	Pellabo			6337312	0396929	Garnet amphibolite
BRO17106	Pellabo			6337817	0397705	Garnet amphibolite
BRO17107	Pellabo			6337904	0397353	Garnet amphibolite, migmatized
BRO17143	Svenslund			633----	039----	Garnet amphibolite

I.II Complete list of localities with coronitic metagabbro.

Coronitic metagabbro						
Locality ID	Locality	Outcrops	Contact	SWEREF99TM N	SWEREF99TM E	Rock type
BRO17075AB	Bassö	A B		6335377	0396036	Metagabbro
BRO17075C	Bassö	C		6335423	0395900	Metagabbro
BRO17091	Bassö			6335693	0396204	Metagabbro
BRO17092	Bassö			6335843	0396341	Metagabbro

I.III Complete list of localities with gneisses and metagranites.

Felsic rocks						
Locality ID	Locality	Outcrops	Contact	SWEREF99 TM N	SWEREF99 TM E	Rock type
BRO17001+	Hästabokärret	01/02		6338077	0392830	gneiss
BRO17003+	Daskebo sten-brott	03/04		6338125	0393280	gneiss pegmatitic
BRO17006A	Vickelsbo	A	X	6337929	0393164	gneiss pegmatitic
BRO17011A	Lalåsen	A	X	6337677	0394493	Granitic gneiss
BRO17012+	Lalåsen	12/13/14		6337703	0394361	gneiss
BRO17018	Björnamossen			6338643	0395155	gneiss pegmatitic
BRO17022A	Stenbrohult	A	X	6337239	0395406	gneiss pegmatitic
BRO17023+	Stenbrohult	23/24/25		6337330	0395168	gneiss pegmatitic
BRO17036	N. Kalvia			6336193	0392840	gneiss pegmatitic
BRO17052ABC	Tovasjötorpet	ABC		6336422	0392858	gneiss pegmatitic
BRO17053	Tovasjötorpet			6336425	0393365	gneiss
BRO17054	Tovasjö			6336609	0392994	gneiss pegmatitic
BRO17055+	V. Hyggås	55AB/56		6336046	0393342	gneiss pegmatitic
BRO17057	Kalvia			633----	039----	gneiss
BRO17058+	V. Hyggås	58/59/60/61/62				gneiss pegmatitic
BRO17064B	V. Hyggås	B	X	6335885	0393583	gneiss
BRO17066	V. Hyggås			6335994	0393825	gneiss pegmatitic
BRO17068B+	Prippebo	68B/69	X	6335846	0394261	gneiss pegmatitic
BRO17071A	N. Bröttjaryd	A	X	6335005	0393513	gneiss
BRO17073ABC+	W. Bröttjaryd	73ABC/76		633----	039----	gneiss
BRO17074ABC	Östra Kalvia	ABC				gneiss
BRO17083	Östra Kalvia			6334806	0392879	gneiss pegmatitic
BRO17080B	Fållen	B	X	6335413	0394127	gneiss
BRO17082	Lillegård			6334055	0396829	gneiss pegmatitic
BRO17083	Östra Kalvia			6334806	0392879	gneiss pegmatitic.
BRO17084	Nabben		X	633----	039----	gneiss pegmatitic., Gneissic granodiorite
BRO17085+	Nabben	85/86		6334456	0397599	gneiss pegmatitic
BRO17087	Nabben			6334564	0397332	gneiss pegmatitic
BRO17088	Nabben			6334380	0396803	gneiss pegmatitic
BRO17089	N. Nabben			6334868	0397368	gneiss pegmatitic
BRO17098+	Norra Stavås	98/99		633----	039----	gneiss pegmatitic
BRO17102	Pellabo			6337356	0397107	gneiss pegmatitic
BRO17103	Pellabo			6337317	0397018	gneiss pegmatitic
BRO17108	Pellabo			6338452	0397385	gneiss pegmatitic
BRO17109	Pellabo			6337567	0397308	gneiss pegmatitic
BRO17110	Västra Kallset			633----	039----	gneiss pegmatitic
BRO17035	Lalåsen			6336376	0393833	Leucocratic granitic gneiss
BRO17090	Lyckorna			6335240	0397427	Gneissic granodiorite

Appendix II.

Map over the most important localities.

For legend and further details see Fig. 2.

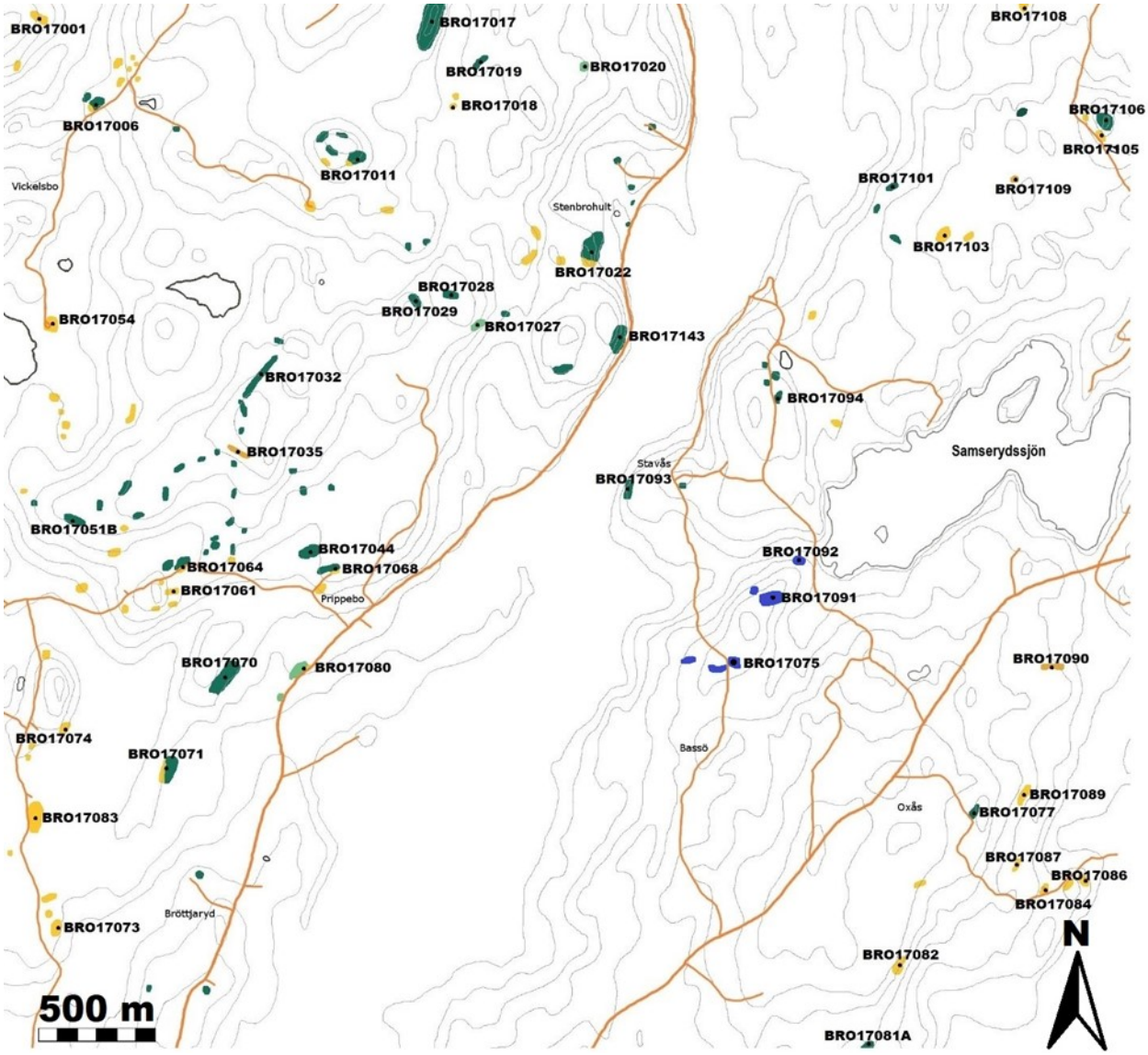

Appendix III.

Thin section data.

Bedrock map over the study area (red box) from SGU (Swedish Geological Survey). Red points mark localities of the analyzed thin sections. The mafic sample JAN040099B is not featured. It is located 55 km west of the area.

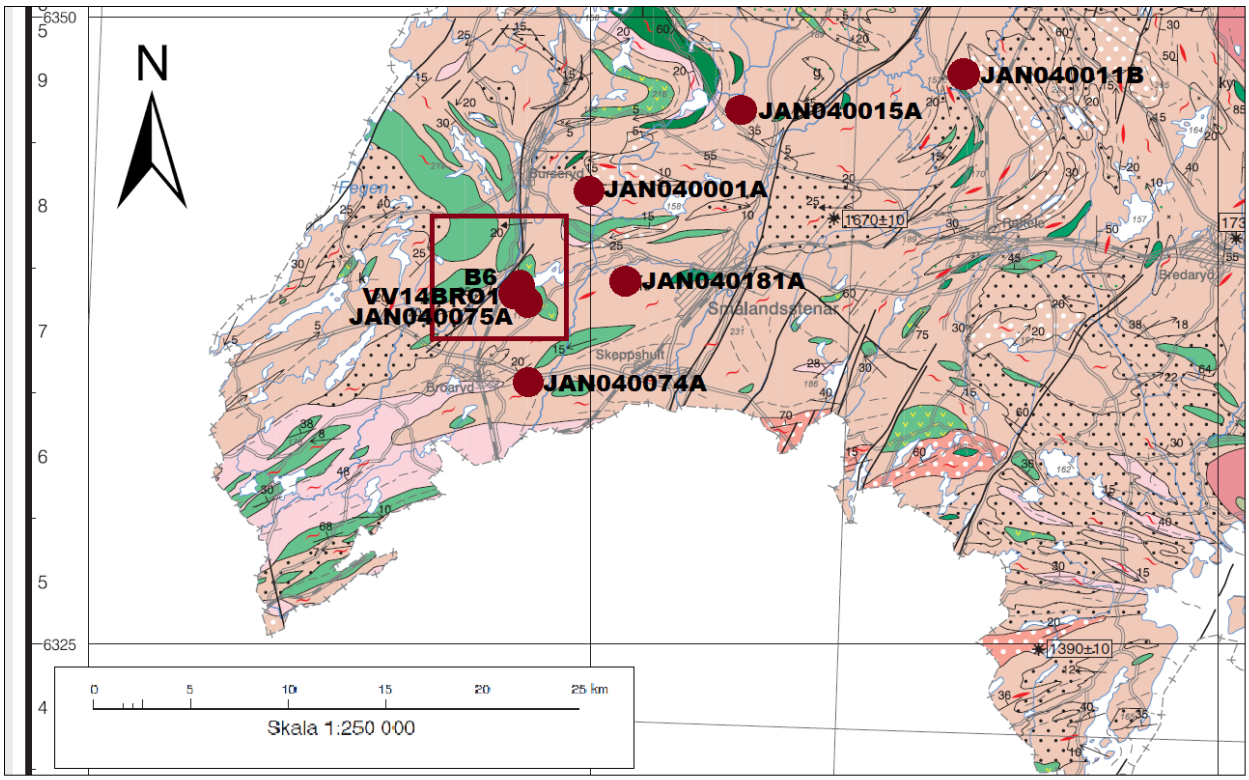

	Sample ID	SWEREF99TM N	SWEREF99TM E	Locality	Rock type
Mafic	JAN040099B	6344998	342995	Hålgryte	Migmatitic garnet amphibo-lite
	JAN040011B	6344119	413305	Nenesmo	Migmatitic garnet-poor amphibolite
	JAN040075A	6335401	396059	Bassö	Coronitic metagabbro
	B6	6335183	396031	Bassö	Coronitic metagabbro
	VV14BRO1	6335184	396034	Bassö	Coronititc metagabbro
Felsic	JAN040001A	6343862	350851	Ma	Migmatitic metagranite
	JAN040015A	6346364	364970	Nennesholm	Migmatitic metagranite
	JAN040074A	6332411	395941	Broaryd	Migmatitic orthogneiss
	JAN040181A	6339525	1351607	SW. Smålands-stenar	Gneissic tonalite-granodiorite, weak foliation.

Appendix IV.
Aeromagnetic anomaly map from the Geological Survey of Sweden (SGU) over the study area (red box).

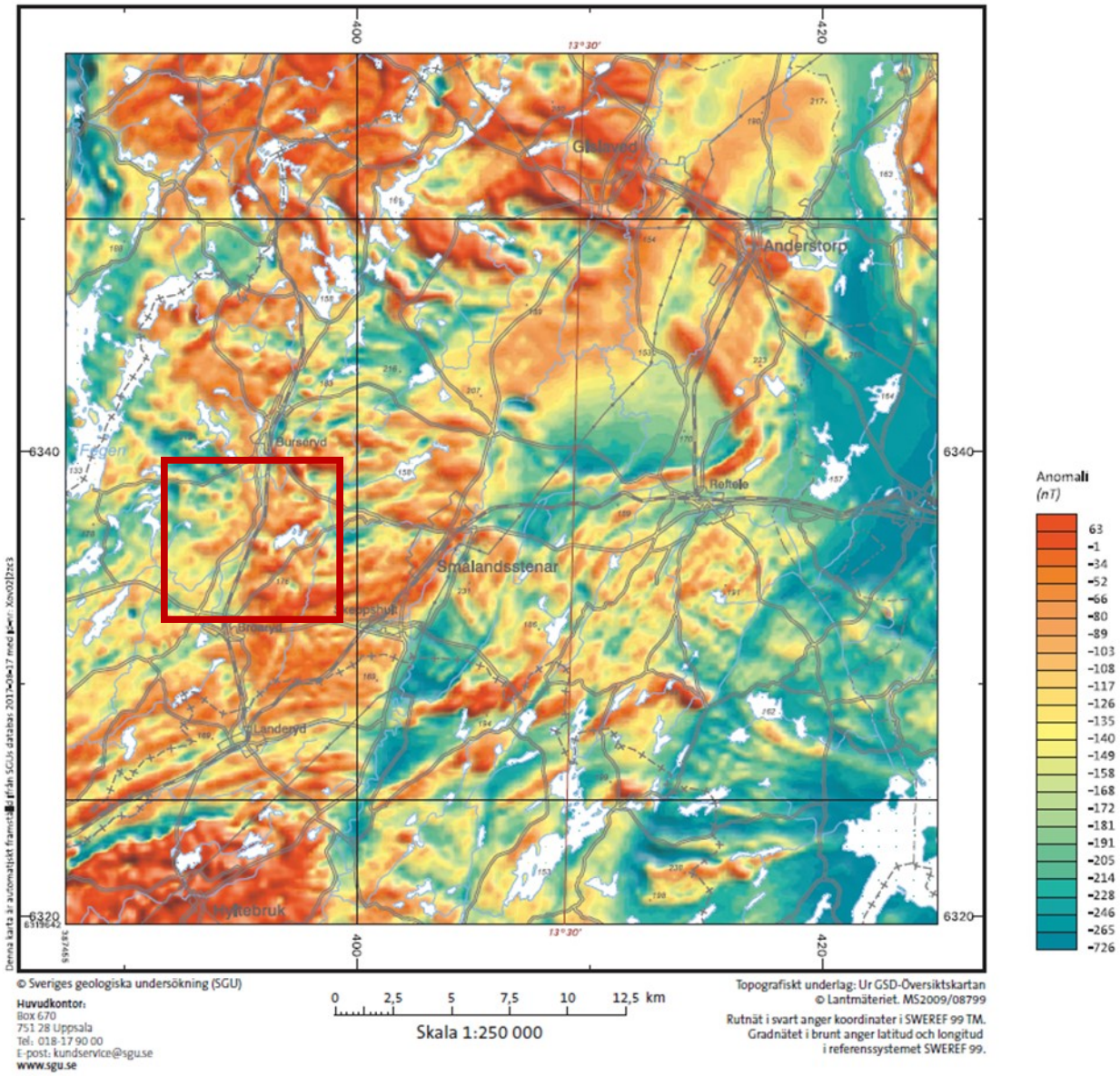

Appendix V.

Composition tables with mineral formula recalculation.

Images show points for selected analyzes, each table has one reference image.

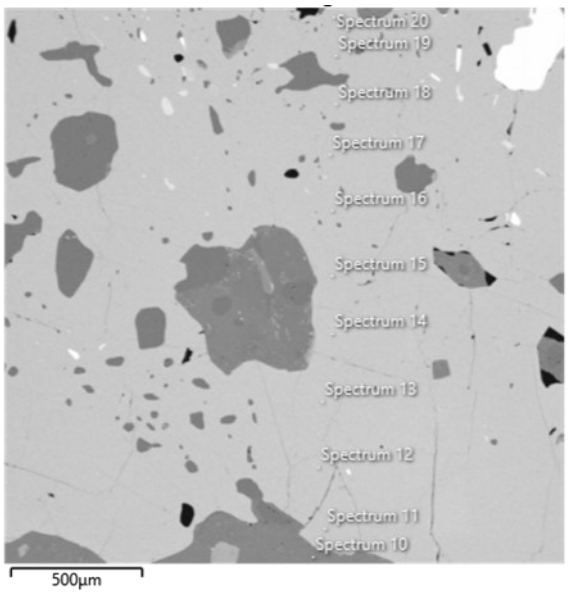

Image V.I. Sample JAN04099B

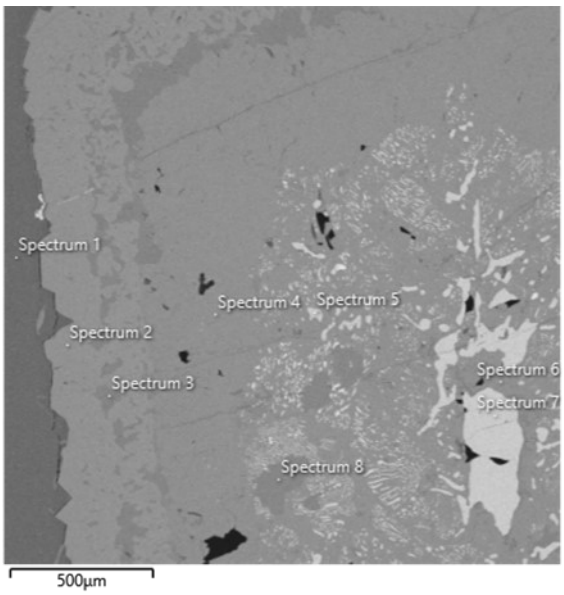

Image V.II. Sample B6

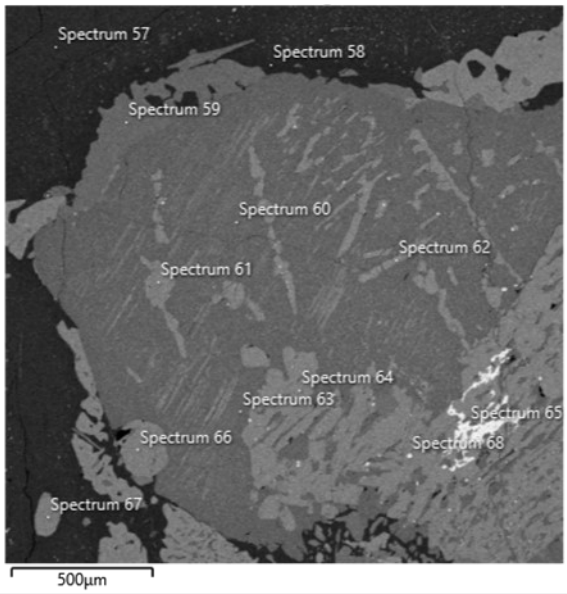

Image V.III. Sample B6

V.I. EDX-analyses of sample JAN04099B. Composition of garnet porpyroblast from rim to core.

Analysis **Sample** **Mineral**	Spectrum 11 JAN04099B Grt	Spectrum 12 JAN04099B Grt	Spectrum 13 JAN04099B Grt	Spectrum 14 JAN04099B Grt	Spectrum 15 JAN04099B Grt	Spectrum 16 JAN04099B Grt	Spectrum 17 JAN04099B Grt	Spectrum 18 JAN04099B Grt	Spectrum 19 JAN04099B Grt	Spectrum 20 JAN04099B Grt
wt%										
SiO_2	37.93	37.84	38.13	37.90	38.14	38.05	38.02	38.06	38.11	38.04
TiO_2	0.07	0.09	0.15	0.03	0.17	0.06	0.01	0.12	0.00	0.01
$Al2O_3$	21.63	21.57	21.52	21.50	21.42	21.78	21.74	21.65	21.90	21.59
FeO	26.42	26.44	25.74	27.24	26.74	26.33	26.68	26.57	26.64	27.33
MnO	1.34	1.65	1.57	1.28	1.20	1.45	1.42	1.34	1.13	1.14
MgO	3.35	2.98	3.16	3.65	3.96	3.63	3.54	3.74	3.95	3.98
CaO	9.25	9.43	9.73	8.40	8.37	8.71	8.58	8.52	8.27	7.90
Total	99.99	100.00	100.00	100.00	100.00	100.00	100.00	100.00	100.00	100.00
Formula based on 12 oxygens										
Si	2.99	2.99	3.00	2.99	3.00	2.99	2.99	2.99	2.99	2.99
Ti	0.00	0.01	0.01	0.00	0.01	0.00	0.00	0.01	0.00	0.00
Al	2.01	2.01	2.00	2.00	1.98	2.02	2.02	2.01	2.02	2.00
Fe	1.74	1.75	1.69	1.80	1.76	1.73	1.76	1.75	1.75	1.80
Mn	0.09	0.11	0.10	0.09	0.08	0.10	0.09	0.09	0.07	0.08
Mg	0.39	0.35	0.37	0.43	0.46	0.42	0.41	0.44	0.46	0.47
Ca	0.78	0.80	0.82	0.71	0.70	0.73	0.72	0.72	0.70	0.67
Total (cation sum)	8.00	8.00	7.99	8.01	8.00	8.00	8.00	8.00	8.00	8.00

V.II. EDX-analyses of sample B6. Garnet corona around pyroxene grain. Orthopyroxene, ilmenite and hornblende symplectite-like texture.

Analysis **Sample** **Mineral**	Spectrum 1 B6 Plg	Spectrum 2 B6 Grt	Spectrum 3 B6 Hbl	Spectrum 5 B6 Ilm	Spectrum 6 B6 Opx
wt%					
SiO_2	56.28	37.81	41.81	0.16	50.85
TiO_2	0.04	-	1.98	49.72	0.31
Al_2O_3	28.02	21.39	12.09	0.02	0.81
FeO	-	29.12	17.42	50.09	31.05
MnO	-	0.93	-	-	-
MgO	-	4.20	10.12	-	16.55
CaO	9.32	6.55	10.91	0.00	0.43
K_2O	0.23	-	1.43	-	-
Na_2O	6.11	-	2.24	-	-
Total	100.00	100.00	98.00	100.00	100.00
Formula based on X oxygens	X = 8	X = 12	X =23	X = 3	X = 6
Si	2.53	2.99	6.18	0.00	1.97
Ti	0.00	-	0.21	0.96	0.01
Al	1.48	1.99	2.11	0.00	0.04
Fe	-	1.92	2.16	1.07	1.01
Mn	-	0.06	-	-	-
Mg	-	0.49	2.23	-	0.96
Ca	0.45	0.55	1.72	0.00	0.02
K	0.01	-	0.27	-	-
Na	0.53	-	0.64	-	-
Total (cation sum)	5.00	8.02	15.52	2.03	4.00

V.III. EDX-analyses of coronitic metagabbro, sample B6. Clinopyroxene grain with orthopyroxene lamellae.

Analysis **Sample** **Mineral**	Spectrum 57 B6 Plg	Spectrum 59 B6 Hbl	Spectrum 60 B6 Cpx	Spectrum 62 B6 Opx	Spectrum 66 B6 Ap	Spectrum 68 B6 Ilm
wt%						
SiO_2	54.65	41.39	51.73	50.88	-	-
TiO_2	-	1.63	-	-	-	48.73
Al_2O_3	29.01	11.54	2.19	0.82	-	-
FeO	1.30	19.99	14.12	33.87	-	51.27
MnO	-	-	-	-	-	-
MgO	-	8.87	10.78	13.91	-	-
CaO	9.38	10.80	19.86	0.51	56.47	-
K_2O	-	1.76	-	-	-	-
Na_2O	5.66	1.98	1.32	-	-	-
F	-	-	-	-	0.01	-
P_2O_5	-	-	-	-	43.52	-
Cl	-	-	-	-	-	-
Total	100.00	98.00	100.00	100.00	100.00	100
Formula based on X oxygens	X = 8	X = 22	X = 6	X = 6	X = 12	X = 3
Si	2.47	5.95	1.97	2.00	-	-
Ti	-	0.18	-	-	-	0.95
Al	1.54	1.96	0.10	0.04	-	-
Fe	0.05	2.40	0.45	1.12	-	1.11
Mn	-	-	-	-	-	-
Mg	-	1.89	0.61	0.82	-	-
Ca	0.45	1.67	0.81	0.02	4.96	-
K	-	0.32	-	-	-	-
Na	0.50	0.55	0.10	-	-	-
S	-	-	-	-	-	-
F	-	-	-	-	0.76	-
P	-	-	-	-	2.92	-
Cl	-	-	-	-	0.04	-
Total (cation sum)	5.01	14.92	4.03	4.00	8.68	2.06

Tidigare skrifter i serien ”Examensarbeten i Geologi vid Lunds universitet”:

496. Mårdh, Joakim, 2017: A geophysical sur-vey (TEM; ERT) of the Punata alluvial fan, Bolivia. (45 hp)
497. Skoglund, Wiktor, 2017: Provenansstudie av detriala zirkoner från ett guldförande alluvium vid Ravlunda skjutfält, Skåne. (15 hp)
498. Bergcrantz, Jacob, 2017: Ett fönster till Kattegatts förflutna genom analys av bottenlevande foraminiferer. (15 hp)
499. O'Hare, Paschal, 2017: Multiradionuclide evidence for an extreme solar proton event around 2610 BP. (45 hp)
500. Goodship, Alastair, 2017: Dynamics of a retreating ice sheet: A LiDAR study in Värmland, SW Sweden. (45 hp)
501. Lindvall, Alma, 2017: Hur snabbt påver-kas och nollställs luminiscenssignaler under naturliga ljusförhållanden? (15 hp)
502. Sköld, Carl, 2017: Analys av stabila iso-toper med beräkning av blandnings-förhållande i ett grundvattenmagasin i Älvkarleby-Skutskär. (15 hp)
503. Sällström, Oskar, 2017: Tolkning av geofysiska mätningar i hammarborrhål på södra Gotland. (15 hp)
504. Ahrenstedt, Viktor, 2017: Depositional history of the Neoproterozoic Visingsö Group, south-central Sweden. (15 hp)
505. Schou, Dagmar Juul, 2017: Geometry and faulting history of the Long Spur fault zone, Castle Hill Basin, New Zealand. (15 hp)
506. Andersson, Setina, 2017: Skalbärande marina organismer och petrografi av tidigcampanska sediment i Kristianstadsbassängen – implikationer på paleomiljö. (15 hp)
507. Kempengren, Henrik, 2017: Föroreningsspridning från kustnära deponi: Applicering av Landsim 2.5 för modellering av lakvattentransport till Östersjön. (15 hp)
508. Ekborg, Charlotte, 2017: En studie på samband mellan jordmekaniska egen-skaper och hydrodynamiska processer när erosion påverkar släntstabiliteten vid ökad nederbörd. (15 hp)
509. Silvén, Björn, 2017: LiDARstudie av glaciala landformer sydväst om Söderåsen, Skåne, Sverige. (15 hp)
510. Rönning, Lydia, 2017: Ceratopsida dinosauriers migrationsmönster under krit-tiden baserat på paleobiogeografi och fylogeni. (15 hp)
511. Engleson, Kristina, 2017: Miljökonsekvensbeskrivning Revinge brunnsfält. (15 hp)
512. Ingered, Mimmi, 2017: U-Pb datering av zirkon från migmatitisk gnejs i Delsjöom-rådet, Idefjordenterrängen. (15 hp)
513. Kervall, Hanna, 2017: EGS - framtidens geotermiska system. (15 hp)
514. Walheim, Karin, 2017: Kvartsmineral-ogins betydelse för en lyckad luminis-censdatering. (15 hp)
515. Aldenius, Erik, 2017: Lunds Geotermisys-tem, en utvärdering av 30 års drift. (15 hp)
516. Aulin, Linda, 2017: Constraining the du-ration of eruptions of the Rangitoto volca-no, New Zealand, using paleomagnetism. (15 hp)
517. Hydén, Christina Engberg, 2017: Drum-linerna i Löberöd - Spår efter flera isrörelseriktningar i mellersta Skåne. (15 hp)
518. Svantesson, Fredrik, 2017: Metodik för kartläggning och klassificering av erosion och släntstabilitet i vattendrag. (45 hp)
519. Stjern, Rebecka, 2017: Hur påverkas luminiscenssignaler från kvarts under laboratorieförhållanden? (15 hp)
520. Karlstedt, Filippa, 2017: P-T estimation of the metamorphism of gabbro to garnet amphibolite at Herrestad, Eastern Seg-ment of the Sveconorwegian orogen. (45 hp)
521. Önnervik, Oscar, 2017: Ooider som naturliga arkiv för förändringar i havens geokemi och jordens klimat. (15 hp)
522. Nilsson, Hanna, 2017: Kartläggning av sand och naturgrus med hjälp av resistivitetsmätning på Själland, Danmark. (15 hp)
523. Christensson, Lisa, 2017: Geofysisk undersökning av grundvattenskydd för planerad reservvattentäkt i Mjölkalånga, Hässleholms kommun. (15 hp)
524. Stamsnijder, Joaen, 2017: New geochronological constraints on the Klipriviersberg Group: defining a new Neoarchean large igneous province on the Kaapvaal Craton, South Africa. (45 hp)
525. Becker Jensen, Amanda, 2017: Den eo-cena Furformationen i Danmark: excep-tionella bevaringstillstånd har bidragit till att djurs mjukdelar fossiliserats.(15 hp)
526. Radomski, Jan, 2018: Carbonate sedimentology and carbon isotope stratigraphy of the Tallbacken-1 core, early Wenlock Slite Group, Gotland, Sweden. (45 hp)
527. Pettersson, Johan, 2018: Ultrastructure and biomolecular composition of sea tur-tle epidermal remains from the Campa-nian (Upper Cretaceous) North Sulphur River of Texas. (45 hp)
528. Jansson, Robin, 2018: Multidisciplinary perspective on a natural attenuation zone in a PCE contaminated aquifer. (45 hp)

529. Larsson, Alfred, 2018: Rb-Sr sphalerite data and implications for the source and timing of Pb-Zn deposits at the Ca-ledonian margin in Swe-den. (45 hp)
530. Balija, Fisnik, 2018: Stratigraphy and pyrite geochemistry of the Lower–Upper Ordovician in the Lerhamn and Fågelsång -3 drill cores, Scania, Sweden. (45 hp)
531. Höglund, Nikolas, 2018: Groundwater chemi-stry evaluation and a GIS-based approach for determining groundwater potential in Mörby-långa, Sweden. (45 hp)
532. Haag, Vendela, 2018: Studie av mikrostrukturer i karbonatslagkäglor från nedslagsstrukturen Charlevoix, Kanada. (15 hp)
533. Hebrard, Benoit, 2018: Antropocen – vad, när och hur? (15 hp)
534. Jancsak, Nathalie, 2018: Åtgärder mot kusteros-ion i Skåne, samt en fallstudie av erosions-skydden i Löderup, Ystad kom-mun. (15 hp)
535. Zachén, Gabriel, 2018: Mesosideriter – redogö-relse av bildningsprocesser samt SEM-analys av Vaca Muertameteoriten. (15 hp)
536. Fägersten, Andreas, 2018: Lateral varia-bility in the quantification of calcareous nannofossils in the Upper Triassic, Aus-tria. (15 hp)
537. Hjertman, Anna, 2018: Förutsättningar för djup-infiltration av ytvatten från Ivösjön till Kristi-anstadbassängen. (15 hp)
538. Lagerstam, Clarence, 2018: Varför svalde svanödlor (Reptilia, Plesiosauria) stenar? (15 hp)
539. Pilser, Hannes, 2018: Mg/Ca i botten-levande foraminiferer, särskilt med avseende på tempe-raturer nära 0°C. (15 hp)
540. Christiansen, Emma, 2018: Mikroplast på och i havsbotten - Utbredningen av mikroplaster i marina bottensediment och dess påverkan på marina miljöer. (15 hp)
541. Staahlnacke, Simon, 2018: En sam-manställning av norra Skånes prekam-briska berggrund. (15 hp)
542. Martell, Josefin, 2018: Shock metamor-phic features in zircon grains from the Mien impact structure - clues to condi-tions during impact. (45 hp)
543. Chitindingu, Tawonga, 2018: Petrological cha-racterization of the Cambrian sand-stone re-servoirs in the Baltic Basin, Swe-den. (45 hp)
544. Chonewicz, Julia, 2018: Dimensionerande vat-tenförbrukning av grundvatten samt alterna-tiva vattenkvaliteter. (15 hp)
545. Adeen, Lina, 2018: Hur lämpliga är de geofy-siska metoderna resistivitet och IP för kart-läggning av PFOS? (15 hp)
546. Nilsson Brunlid, Anette, 2018: Impact of sout-hern Baltic sea-level changes on land-scape development in the Verkeån River valley at Haväng, southern Sweden, dur-ing the early and mid Holocene. (45 hp)
547. Perälä, Jesper, 2018: Dynamic Recrystal-lization in the Sveconorwegian Frontal Wedge, Småland, southern Sweden. (45 hp)
548. Artursson, Christopher, 2018: Stratigra-phy, sedimentology and geophysical as-sessment of the early Silurian Halla and Klinteberg formations, Altajme core, Got-land, Sweden. (45 hp)
549. Kempengren, Henrik, 2018: Att välja den mest hållbara efterbehandlingsmetoden vid sane-ring: Applicering av beslutsstödsverktyget SAMLA. (45 hp)
550. Andreasson, Dagnija, 2018: Assessment of using liquidity index for the approxi-mation of undrained shear strength of clay tills in Scania. (45 hp)
551. Ahrenstedt, Viktor, 2018: The Neoprote-rozoic Visingsö Group of southern Swe-den: Litho-logy, sequence stratigraphy and provenance of the Middle Formation. (45 hp)
552. Berglund, Marie, 2018: Basaltkuppen - ett spel om mineralogi och petrologi. (15 hp)
553. Hernnäs, Tove, 2018: Garnet amphibolite in the internal Eastern Segment, Sveconor-wegian Province: monitors of metamorphic recrystallization at high temperature and pressure during Sveconorwegian orogeny. (45 hp)

LUNDS UNIVERSITET

Geologiska institutionen
Lunds universitet
Sölvegatan 12, 223 62 Lund